Computational study on the influence of nozzle eccentricity in spray formation by means of Eulerian Σ - Y coupled simulations in diesel injection nozzles

F. J. Salvador[a,*], J. M. Pastor[a], J. De la Morena[a], E. C. Martínez-Miracle[a]

[a]*CMT-Motores Térmicos, Universitat Politècnica de València, Camino de Vera s/n, Valencia E-46022, Spain*

Abstract

The present work analyses the effect of the eccentricity of diesel nozzle orifices over the spray behaviour by means of CFD simulations. Several orifice geometries with varying horizontal eccentricity (from 0.50 to 0.94) are selected. Their performance is assessed at a high injection pressure of 200 MPa, a 3 MPa back-pressure and non-evaporative conditions. The nozzle flow characteristics, including cavitation modelled by a Homogeneous Relaxation Model (HRM), are accounted for in the spray performance by means of a Σ - Y model. The code is validated via two reference nozzles, the so called "Spray A" of the Engine Combustion Network plus a second nozzle from a production injector, and then extended to the eccentric geometries. The results and discussions include spray angle and penetration, air entrainment and flow parameters of the nozzle inner conditions versus the eccentricity value.

Keywords: Sigma - Y model, HRM, eccentricity, diesel, spray, atomization

1. Introduction

As the standards applied to combustion engines emissions become more stringent, the need to produce cleaner combustion systems compatible with future climatic requirements is critical. Diesel engines have been widely used thanks to their potential to reduce CO_2 emissions, one of the most significant contributors to global warming effect. However, concerns about their capability to meet future NO_x and particulate matter emissions regulations have arisen over the last years. Even if these pollutants can be substantially reduced by means of aftertreatment systems (such as Diesel Particulate Filters -DPF-, Lean-NOx Trap-LNT- or Selective Catalytic Reactors -SCR-), the origin of the emissions must be also controlled in order not only to reduce them, but also to keep under control the cost, size, durability and fuel consumption impact of the aforementioned elements. While Exhaust Gas Recirculation (EGR) can be used to mitigate NO_x emissions thanks to the lower combustion temperature, its usage is limited due to the subsequent increase of the particulate matter (mainly composed of soot). However, soot formation is controlled by the air-fuel mixing process, which is mainly a result of the injection pressure and the morphology of the injector and chamber geometry (Arai, 2012; Heywood, 1988; Lefebvre, A., McDonell, 2017). Additionally, the fuel-air mixing controls the combustion timing and duration, affecting the indicated efficiency, as well as the flame distance to the cylinder walls, impacting heat transfer losses.

Since the 1970's the study of the parameters that characterize the spray performance has been a constant research topic with the aim of increasing efficiency while reducing emissions. First works by Wakuri et al. (1960), the extensive studies by Hiroyasu et al. (Hiroyasu, 2000; Hiroyasu and Arai, 1990; Hiroyasu and Kadota, 1974; Hiroyasu and Miao, 2003) and several others like Reitz et al. (Reitz, 1987; Reitz and Bracco, 1982; Reitz and Diwakar, 1987) postulated the importance of the spray mechanics, specially the relationship between the tip

*Corresponding author

Email addresses: fsalvado@mot.upv.es (F. J. Salvador), jopasen@mot.upv.es (J. M. Pastor), joadela@mot.upv.es (J. De la Morena), enmarmuo@mot.upv.es (E. C. Martínez-Miracle)

Preprint submitted to Elsevier *April 23, 2020*

Nomenclature

A	Area
a	Ellipse semi-major axis
AMR	Adaptive Mesh Refinement
b	Ellipse semi-minor axis
c	Focal length
C_a	Area coefficient
C_d	Discharge coefficient
C_v	Velocity coefficient
C_Σ	Model coefficient for Σ
D	Mass diffusion coefficient
D_o	Nozzle outlet diameter
D_Σ	Diffusion coefficient for Σ
D_{eq}	Equivalent diameter, defined as $D_{eq} = D_o\sqrt{\frac{\rho_f}{\rho_a}}$
e	Eccentricity
e	Specific energy
F	Cavitation parameter of the HRM model
h	Enthalpy
HRM	Homogeneous Relaxation Model
$\bar{k}$	Turbulent kinetic energy
K	Temperature diffusion coefficient
$\dot{M}_f$	Momentum flux
$\dot{m}_f$	Mass flow
M	Momentum
m	Mass
P	Pressure
PMD	Projected mass density
R	Radio
r_{eq}	Equivalent droplet radio
$RANS$	Reynolds Averaged Navier-Stokes equations
RNG	Re-normalization Group
S_i	Source term
Sc	Schmidt number
T	Temperature
$\tilde{u_i}$	Velocity component
u_{eff}	Effective velocity
u_{th}	Theoretical velocity
V	Volume
XY_{plane}	Perpendicular to the ellipse major axis
$\bar{Y}$	Liquid volume fraction
$\tilde{Y}$	Liquid volume fraction, Favre averaged
Y	Mass fraction
ZY_{plane}	Perpendicular to the ellipse minor axis
α	Void fraction
α_1	Calibration parameter
α_2	Calibration parameter
δ_{ij}	Kronecker delta
$\bar{\epsilon}$	Turbulent energy dissipation
φ	Non-dimensional pressure ratio
μ	Viscosity
μ_t	Turbulent viscosity
ν_T	Kinematic turbulent viscosity
ρ	Global density
Σ	Surface are density
σ_{ij}	Viscous stress tensor
θ	Time scale factor

penetration, the spray angle and the air entrainment. Different optical diagnostics have been developed to evaluate the primary atomization and initial spray formation process (Desantes et al., 2011; Dumouchel, 2008; Manin et al., 2014), the fuel-air mixing (Espey et al., 1997; Schulz and Sick, 2005) and the combustion development (Desantes et al., 2018; Idicheria and Pickett, 2011). The evolution of computational fluid dynamics in the recent years has made possible to study in further details the importance of the nozzle geometry in the atomization process (Anez et al., 2018; Desjardins and Pitsch, 2010; Salvador et al., 2014, 2015b). In this sense, approaches such as the $\Sigma - Y$ model (Vallet and Borghi, 1999; Vallet et al., 2001) which allows a coupled flux between nozzle and spray through a Eulerian-Eulerian simulation (Desantes et al., 2016a; Wang et al., 2011; Xue et al., 2015). In this model, flux phases are considered as a pseudo-fluid inside a single velocity field. This method introduces the possibility of simulate cavitation phenomena if the geometry is prone to cavitate. In this sense, several authors such as Zhao et al. (2014) and Battistoni et al. (2015) used an Homogeneous Relaxation Model to evaluate cavitation phenomena in nozzles.

Already decades ago, works by Sforza et al. (1966) and Trentacoste and Sforza (1967) made first approximations to the aspects of jets produced by elliptical nozzles. Hussain et al. (Husain and Hussain, 1991; Hussain and Husain, 1989) and Ho and Gutmark (1987) analysed also these jets from a theoretical perspective. More recently, studies about elliptical nozzles applied to spray mechanics revealed that this particular shape was able to improve the general dispersion of the injected fluid (Yunyi et al., 1998). Lee et al. (2006) performed comparisons between elliptical and cylindrical single-hole nozzles and found an improved spreading angle, specially in the plane corresponding to the minimum diameter. Similar results were reported by Yu et al. (2018), showing a lower penetration in favour of a wider angle and then a greater atomization effect associated to elliptical single-hole nozzles. Hong et al. (2010) studied cavitation phenomena inside transparent elliptical nozzles, concluding that longer cavitation fields (up to the orifice outlet) were appearing. Based on the work by Hong et al., Ku et al. (2011) applied CFD techniques in order to verify the relationship between the internal flow and the behaviour of the spray. Their investigation showed how cavitation takes place in the major axis limits due to a greater contraction of the stream-lines in that zone for single-hole nozzles. The internal profiles of the CFD simulations related the turbulence subjected to cavitation to a greater spreading angle in the major axis plane. Finally, some approximations to real diesel engines were made by Matsson and Andersson (2002), accounting the impact on emissions of elliptical geometries, with a general decrease of NO_x emissions and fuel consumption for elliptical geometries, but with varying smoke production depending on the aspect ratio value.

Despite the previous works describe some of the physics related to the impact of elliptical orifices on nozzle flow and spray formation, most of them may not be fully representative from a practical point of view. On the one hand, most of the studies are performed for single-hole axi-symmetric nozzles. However, diesel engines require multi-orifice nozzles, which are affected by the change of direction of the flow induced by the inclination of the orifices' axis compared to the injector. On the other hand, nozzle sizes within literature are usually larger than a representative diesel nozzle ($< 0.2mm$). A first approach to this more complex problem was described by Molina et al. (2014). In their work, several detailed CFD simulations were carried out in order to clarify how the internal flow of a common rail diesel injector with elliptical orifices could affect the atomization, and an extrapolation to the effects in the spray characteristics was made based on a theoretical reasoning. The present paper intends to get a deeper view into the effects of elliptical nozzles over the spray by means of advanced coupled internal-external flow simulations. This will also allow to understand some of the effects described in the literature. On the basis of a cavitating cylindrical nozzle whose hydraulic behaviour is known, six elliptical geometries have been modelled. The horizontal radius has been gradually increased inducing eccentricity levels from 0.5 to 0.94, maintaining a constant outlet section, while the rest of the geometrical morphology has been kept as in the original nozzle. The validation of the computational model has been carried out following two lines of action. First, a non-cavitating single-hole nozzle from the Engine Combustion Network (https://ecn.sandia.gov/ecn-data search/), named Spray A, has been evaluated in terms of mass flow rate, momentum flux, spray angle and projected mass density. Then, a Homogeneous Relaxation Model (HRM) used to predict cavitation performance has been assessed against hydraulic experimental data from a cylindrical multi-hole nozzle, which is the same used as baseline for the rest of the study. Once the models are validated, the performance of the elliptical nozzles is analysed in terms of the flow conditions at the nozzle outlet (mass flow, momentum flux, liquid and vapour fractions, radial and axial velocity profiles, etc), as well as spray features (such as the spray angle, the air entrainment and the spray tip penetration). Several discussions over the information available in literature have been exposed and the behaviour of the simulations have been clarified.

The investigation has been divided into six sections. Section 2 introduces the computational model, while section 3 describes the employed methodology. It includes the description of the models, the geometries, fluid properties and the post-process and comparison techniques. Section 4 discusses the validation of the model, including the description of the nozzle geometries used for this purpose (Spray A and a production multi-hole injector), the characteristics of the meshes and model constants configuration used. Section number 5 shows the results for the six nozzles elliptical geometries considered. All the nozzles have been compared relating their spray characteristics with the previous literature findings, paying special attention to coherence between extracted properties at the nozzle outlet and the spray behaviour. The last section collects the main conclusions of the present work.

2. Model description

The coupling between the nozzle internal flow and the spray is made by means of a $\Sigma - Y$ atomization model. In this formulation, all the phases are treated as a pseudo-fluid with an unique velocity field for vapour fuel, liquid fuel and chamber gas (Desantes et al., 2016a; Pandal Blanco, 2016). This approximation assumes that the exiting spray is characterised by large values of Reynolds and Webber numbers. From this point of view, bigger scales of turbulence can be transported, while small unresolved scales are computed using standard closure models. The dispersion of the liquid phase is then traced by means of a scalar function. This magnitude takes a value of 1 when only liquid exists, and 0 if there is only vapour phase. The transport equation for the liquid mass fraction on its Favre averaging form is:

$$\frac{\partial \bar{\rho}\tilde{Y}}{\partial t} + \frac{\partial \bar{\rho}\ \tilde{u}_i \tilde{Y}}{\partial x_i} = 0, \tag{1}$$

where $\bar{\rho}$ denotes the density, $\tilde{u}$ the axial velocity, x the axial position and $\tilde{Y}$ is the mean mass-averaged volume fraction defined as:

$$\tilde{Y} = \frac{\overline{\rho_{liq} Y}}{\bar{\rho}}. \tag{2}$$

$\bar{Y}$ being the volume fraction.

If an immiscible mixture is assumed for the two phases, the relation between the mass-averaged value of the liquid volume fraction can be related to the density by:

$$\frac{1}{\bar{\rho}} = \frac{\tilde{Y}}{\rho_l} + \frac{1-\tilde{Y}}{\rho_g}. \tag{3}$$

An equation of state is then assigned to each phase:

$$\rho_g = \frac{P}{R_g T}, \tag{4}$$

$$\rho_l = f(p, T). \tag{5}$$

The energy transport equation only accounts the internal energy of the fluid, and stands as follows:

$$\frac{\partial \bar{\rho} e}{\partial t} + \frac{\partial \tilde{u_j} \bar{\rho} e}{\partial x_j} = -P\frac{\partial \tilde{u_j}}{\partial x_j} + \sigma_{ij}\frac{\partial \tilde{u_i}}{\partial x_j} + \frac{\partial}{\partial x_j}\left(K\frac{\partial T}{\partial x_j}\right) + \frac{\partial}{\partial x_j}\left(\bar{\rho} D \sum_m h_m \frac{\partial \tilde{Y_m}}{\partial x_j}\right), \tag{6}$$

Where Y_m and h_m are the mass fraction and enthalpy for each species respectively, D is a mass diffusion coefficient, P is the pressure, σ_{ij} the stress tensor, e is the specific energy and T is the temperature. The relation between the different species is given by:

$$h(T) = \tilde{Y} \cdot h_l(T) + (1-\tilde{Y}) \cdot h_g(T). \tag{7}$$

The turbulent term in the liquid mass transport is modelled as

$$\bar{\rho}\widetilde{u_i' Y'} = \frac{\mu_t}{Sc}\frac{\partial \tilde{Y}}{\partial x_i}. \tag{8}$$

Subsequently, the momentum conservation equation can be written as:

$$\frac{\partial \bar{\rho}\tilde{u}_i}{\partial t} + \frac{\bar{\rho}\tilde{u}_i\tilde{u}_j}{\partial x_j} = -\frac{\partial P}{\partial x_i} + \frac{\partial \sigma_{ij}}{\partial x_j} + S_i, \tag{9}$$

where σ_{ij} denotes the viscous stress tensor, equals to:

$$\sigma_{ij} = \mu\left(\frac{\partial \tilde{u_i}}{\partial x_j} + \frac{\partial \tilde{u_j}}{\partial x_i}\right) + \left(\frac{2}{3}\mu\frac{\partial \tilde{u_k}}{\partial x_k}\delta_{ij}\right), \tag{10}$$

μ is representing the viscosity and δ_{ij} is the Kronecker delta.

Finally, the interphase surface area density is defined as the quantity of spatial surface per unit volume (Ishii and Hibiki, 2006; Vallet and Borghi, 1999). Hence, the transport equation associated to this scalar magnitude is:

$$\frac{\partial\tilde{\Sigma}}{\partial t}+\frac{\partial\tilde{u_j}}{\partial x_j}-\frac{\partial}{\partial x_j}\left(D_\Sigma\frac{\tilde{\Sigma}}{\partial x_j}\right)- C_\Sigma\tilde{\Sigma}\left(1-\frac{\tilde{\Sigma}}{\Sigma_{eq}}\right)-S_{\Sigma_{evap}}-S_{\Sigma_{init}}=0, \quad (11)$$

where

$$\overline{\Sigma_{eq}}=\frac{3\bar{\rho}Y}{\rho_l r_{eq}}, \quad (12)$$

$$S_{\Sigma_{evap}}=\frac{2\Sigma}{3\bar{Y}}S_{evap}, \quad (13)$$

$$C_\Sigma=\alpha_1\frac{\tilde{\varepsilon}}{\tilde{k}'}, \quad (14)$$

$$r_{eq}=\alpha_2\frac{\sigma^{3/5}}{\tilde{\varepsilon}^{2/3}}\frac{(\bar{\rho}\tilde{Y})^{2/15}}{\rho_l^{11/15}}, \quad (15)$$

$$D_\Sigma=\frac{\nu_T}{Sc_\Sigma}. \quad (16)$$

D_Σ is a diffusion coefficient, Y is the volume fraction of fuel, $S_{\Sigma_{evap}}$ is a source term related to vaporization, $S_{\Sigma_{init}}$ is the initialization value, r_{eq} is the equilibrium radius for virtual droplets. Finally, α_1 and α_2 are model parameters subjected to calibration. The terms above can be used to calculate equivalent droplet sizes as part of the transition chain to parcels in an hybrid Eulerian-Lagrangian model. Although this kind of comparison is beyond the limits of this paper, it is a good indication of the potential of the model.

$$S_{\Sigma_{init}}=\frac{\Sigma_{min}-\Sigma}{\Delta t}pos(\Sigma_{min}-\Sigma), \quad (17)$$

$$\Sigma_{min}=\sqrt{\alpha(1-\alpha)}V^{1/3}, \quad (18)$$

$$pos(\Psi)=\begin{cases}1 & \text{if } \Psi>0\\ 0 & \text{if } \Psi\leq 0.\end{cases} \quad (19)$$

In diesel engines, usual values for α_1 and α_2 are respectively 1 and 4 (Vallet et al., 2001; Wang et al., 2011). For a deeper mathematical explanation of the model and coefficients, previous work by Pandal Blanco (2016) can be consulted.

As stated during the introduction, the mass transfer between fuel vapour and liquid phase due to cavitation is modelled by a Homogeneous Relaxation Model (HRM) (Bilicki and Kestin, 1990; Shields et al., 2011). The model assumes that the rate at which the instantaneous mass (x) approaches its equilibrium value ($\bar{x}$) depends on a time scale factor (θ) or relaxation factor. The linear relation is expressed as:

$$\frac{D_x}{Dt}=\frac{\bar{x}-x}{\theta}. \quad (20)$$

Two time scales are calculated, one for evaporation and another for condensation:

$$\theta_E=\theta_0\alpha^{-0.54}\varphi^{-1.76}, \quad (21)$$

$$\theta_C=F\theta_0\alpha^{-0.54}\varphi^{-1.76}. \quad (22)$$

Notice that α is the void fraction, equals to $(1-\bar{Y})$. The value of θ_0 is set to $3.84e-7s$ and φ is the non-dimensional pressure ratio.

$$\varphi=\frac{P_{sat}-P}{P_c-P_{sat}}, \quad (23)$$

where P_c denotes the critical pressure of the fluid. In equation 22, F has a value of 5000 according to the conclusions from previous analysis by He et al. (2017).

3. Methodology

The current study is divided in two steps. First, two existing injector nozzle geometries are used for the validation of the simulations in terms of the internal flow characteristics and the spray formation processes. The internal flow is validated based on hydraulic data from a multi-hole nozzle, characterized by cylindrical orifices so that cavitation is induced. For the validation of the spray models, the so called "Spray A" from the Engine Combustion Network (ECN) (https://ecn.sandia.gov/ecn-data search/), which is a single-hole conical nozzle, is selected. The advantage of this nozzle is that it is widely characterised in terms of the spray evolution by different experimental techniques.

Later on, the impact of the eccentricity in the outlet section of the nozzle is analysed. For this purpose, six different 3D nozzle geometries with increasing levels of eccentricity have been explored for this study (Table 1), using as a basis the geometry from a production 6-hole diesel nozzle. The initial dimensions of this injector were characterized using silicone moulds. This method was widely used in similar studies, providing a geometrical error about 2% in the main nozzle magnitudes (Macian et al., 2003; Payri et al., 2016, 2011; Salvador et al., 2018a,b). The whole internal geometry of the real injector, including the needle seat, sac, the hydrogriding radius and the outlet section, has been replicated for all the six elliptical nozzles. Even though the outlet area of the orifice remains constant, the nozzle shape varies as the minor radius (axial with respect to the injector body axis) decreases and the major one (tangential to the injector) increases (see Figure 1a and 1b for further details). The outlet orifice has been defined taking into account the expressions below:

$$A_{ellipse} = \pi ab = D^2_{base}\frac{\pi}{4}\mu m^2, \tag{24}$$

$$\text{being} \qquad a = \frac{A}{R_{min}\pi}, \tag{25}$$

$$\text{and} \qquad e = \frac{c}{a}. \tag{26}$$

Where a is the minor radius, b is the major radius and c is the so-called linear eccentricity:

$$c = \sqrt{a^2 - b^2}. \tag{27}$$

Radius [μm] and eccentricities		
R_{min} **(b)**	R_{max} **(a)**	e
80	90.31	0.50
75	96.33	0.62
70	103.21	0.73
65	111.15	0.81
55	131.36	0.90
50	144.5	0.94

Table 1: Geometries used for the study.

(a) $eccentricity = 0.50$ (b) $eccentricity = 0.94$

Figure 1: 3D geometry models

In order to ensure the independence of the results from the computational boundaries, a $30 \times 30mm$ chamber domain has been chosen for the injection process (Figure 2). The symmetry of the problem allows to calculate a single 60° sector of the injector, corresponding to one nozzle orifice, reducing the computational effort. Turbulence is modelled by unsteady Reynolds-Averaged Navier-Stokes (U-RANS) methodology, employing a Favre-averaged formulation for compressible fluids. Given the high flow velocity and the expected appearance of cavitation, Reynolds values higher than 20000 have been estimated, so a turbulent flow is expected inside the nozzle. For this reason, a standard $k - \epsilon$ model (Launder and Sharma, 1974; Launder and Spalding, 1974) has been selected as a turbulence model. Although this particular approach performance is known to be worse than others like the $k-\omega$ in recirculation zones (such as those generated in cavitation problems) and low-Reynolds-number flows (David C.Wilcox, 1994), it has commonly produced better results in free stream flow conditions (David C.Wilcox, 1994). The Re-Normalisation Group (RNG) $k-\epsilon$ (Yakhot and Smith, 1992) model was also proposed since it helps to overcome some of the numerical problems induced by separated flows. However, several studies using the $\Sigma - Y$ model found in literature use the standard $k - \epsilon$ model for similar purposes as the current study, with a modified value for the $C_{\epsilon 1}$ coefficient equals to 1.6 instead of 1.44 (Dally et al., 1998; Garcia-Oliver et al., 2013; Hoyas et al., 2013; Janicka and Peters, 1982; Pandal Blanco, 2016; Pope, 1978; Xue et al., 2015). Therefore, this last configuration has been taken to ensure consistency with previous works.

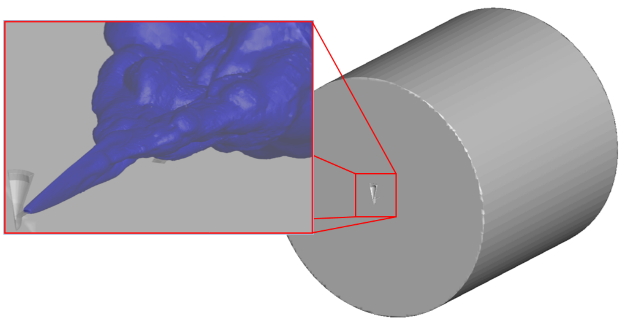

Figure 2: Simulated domain, $30 \times 30mm$

The energy equation has been solved in its internal form. As already introduced, a Homogeneous Relaxation Model (HRM) (Bilicki et al., 1996; Bilicki and Kestin, 1990; Brusiani et al., 2013; Downar-Zapolski et al., 1996; Schmidt, 1997; Schmidt et al., 2010) has been chosen in order to solve the cavitation generated at the nozzle inlet in the multi-hole geometries. In this zone, the accelerating fuel detaches from near walls and produces local pressure drops. This phenomenon depends on the injection pressure, the back-pressure and the nozzle geometry (Arcoumanis et al., 2000; López et al., 2017; Payri et al., 2005, 2004b; Salvador et al., 2015a, 2017; Soteriou et al., 2010; Sun et al., 2015). The geometries under study are expected to cavitate since none of them are conical. The effect of cavitation requires a small time step in order to reach convergence. This issue limits the total time of injection to 500 μs, performed at full needle lift conditions.

Regarding the boundary conditions, chamber outlet far boundaries (bottom circular plane and peripheral curved surface) are set as outflow conditions with zero normal gradient for the velocity. The inlet boundary at the nozzle has been defined in terms of a static pressure. A wall function has been applied to all wall boundaries. For reference nozzles, the injection parameters match the ECN target conditions (https://ecn.sandia.gov/ecn-data search/) in non-evaporative experiments. On the other hand, the elliptical nozzles have been simulated at 200 MPa injection pressure and 3 MPa back-pressure, with an initial temperature of 303 K. Table 2 summarizes all the applied conditions.

Boundary conditions, $P[MPa]$, $T[K]$				
Nozzles	P_{inj}	P_{back}	T_f	T_c
Spray A	150	2	343	303
Elliptical	200	3	303	303

Table 2: CFD boundary conditions.

A transverse mass criteria has been chosen in order to calculate the angle. As the results produced by the software are provided in an *OctreeMesh* (Senecal et al., 2011), a Cartesian mesh with a 50 μm resolution is generated and adjusted to the domain for the first 20 mm (Figure 3a). Variables are then parallel interpolated for post-processing.

The transverse mass is then calculated according to the summation of the liquid mass in two planes projection XY (minor radius) and ZY (major ra-

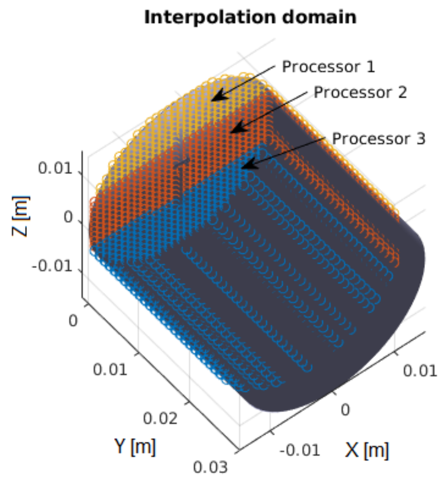

(a) Angle calculation, virtual mesh generation.

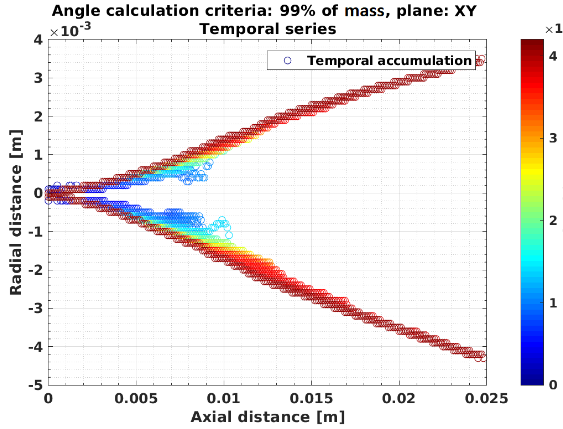

(b) Points for CFD angle calculation, Spray A

Figure 3: CFD angle calculation methodology.

dius), (see Figure 3b).

$$m_{liquid} = \sum_{i=1}^{n} \overline{\rho}_i \tilde{Y}_{f_i} V_{mesh}. \quad (28)$$

Then, for each transverse integrated slice, the spray limits are calculated according to a certain percentage in mass (95 or 99%) of the total mass contained in each axial slice.

Following the normalized path suggested by the ECN, N-dodecane fluid and vapour tabulated properties have been used within the reference nozzle simulations. Vapour and nitrogen have been treated as ideal and compressible gases, while N-dodecane is set as dependent on temperature and pressure. With respect to the elliptical nozzles, a commercial diesel fuel has been chosen as working fluid and has also been characterized as a function of temperature and pressure. Temperature correlations have been implemented in a tabulated format while compressibility effect is taken into account by the compressibility modulus ($B = 1.49e9$ MPa). More details about how each of the main fuel properties is considered and the literature works from which the information was extracted can be seen in Table 3.

Property	**Value or function**
Density	$825.5\Delta e^{\frac{P-P_{ref}}{B}}$ [1]
Viscosity	$f(T, P_{ref})$ [1,2]
Vapour pressure	$f(T, P_{ref})$ [3]
Surface tension	$0.029 N/m$ [4]
Specific heat (C_p)	$f(T, P_{ref})$ [3]
1-Desantes et al. (2015)	
2-Salvador et al. (2018a)	
3-Kolev (2012)	
4-Dechoz and Rozé (2004)	

Table 3: Diesel fuel main properties ($P_{ref} = 0.1$ MPa).

4. Model validation

Two kinds of validation have been performed in this study. On the one hand, coupled nozzle-spray model (Σ - Y) has been compared to an extensive dataset available in the literature for Spray A (injector #210675) from the Engine Combustion Network group (https://ecn.sandia.gov/ecn-data search/), which represents a conical (non-cavitating, HRM model not included) single-hole and almost axi-symmetric geometry. On the other hand, a partial validation of the injection process with cavitation has been performed based on nozzle internal flow experimental data for a cylindrical multi-hole nozzle, whose internal geometry and inner flow parameters have been previously characterised. All the models listed above have been configured within the software CONVERGE CFD (https://convergecfd.com).

Validation of single-hole Spray A

Figure 4a shows the geometry of the Spray A nozzle, which as previous said represents a single-hole quasi-axi-symmetric layout with a slight deviation of the nozzle from the main jector body axis. Since this deviation barely affects the spray performance, it is commonly considered axi-symmetric. The 3D geometry has been acquired from the *x-ray* measurements provided in the ECN data base (Kastengren et al., 2012). The nominal diameter is measured at 90 μm and the nozzle exhibits a *k-factor* of 1.5 (Macian et al., 2003).

The chosen mesh configuration provides a minimum of fifteen rows of cells inside the nozzle, representing an average of 6 μm. Some authors have established a minimum of ten cells as a good approach (Garcia-Oliver et al., 2013; Lebas et al.; Xue et al., 2015).

Cell size [μm]	
Mesh region	**Spray A**
Base size	384
Nozzle	6
Near nozzle spray	12 (up to 5 mm)
Needle	48
AMR u (nozzle)	Disabled
AMR α (nozzle)	Disabled
AMR u (spray)	24
Total cells	$\sim 9e6$

Table 4: Mesh configuration for Spray A

Figures 4b and 4c show the computational mass flow and momentum flux at the nozzle outlet together with the experimental ones, extracted from the literature (Pickett et al., 2011, 2013). Despite the experimental data is obtained from a transient injection process, while the simulations are made at steady maximum needle lift, it can be noted that a good agreement between steady-state parts of the injection is reached for either mass flow rate (Figure 4b) or momentum flux (Figure 4c).

The spray angle calculation has been carried out following the methodology in section 2, computing an average angle of 19.1° for the 99% of the projected radial mass and 14.6° for the 95% in mass (Figure 5b). The interpolation of the angle has been conducted over the first 20 mm of the simulation discharge chamber. Mean angle values were calculated over the steady part of the simulation (> 300 μs). The experimental angle data is available in previous works (Pickett et al., 2011, 2013) based on Diffused Back-Light (DBI) visualisation tests. Figure 5a shows the fitting lines for an experimental angle up to 20 mm axial distance from

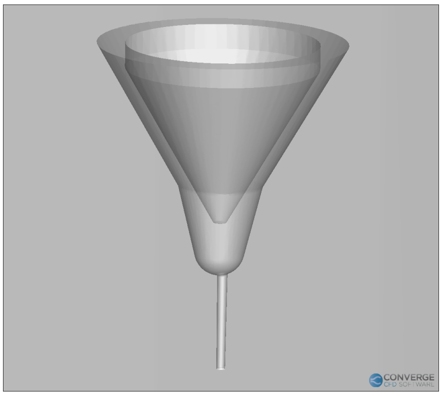

(a) Spray A, 3D geometry

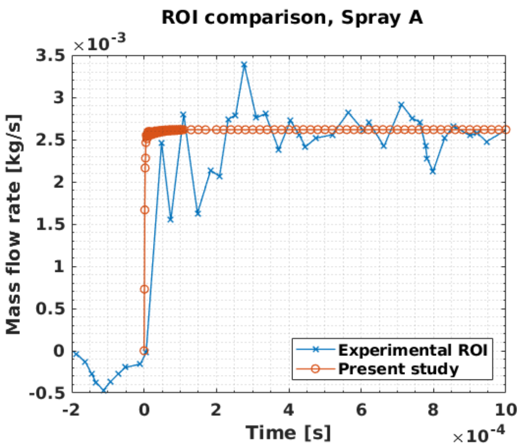

(b) Rate of injection

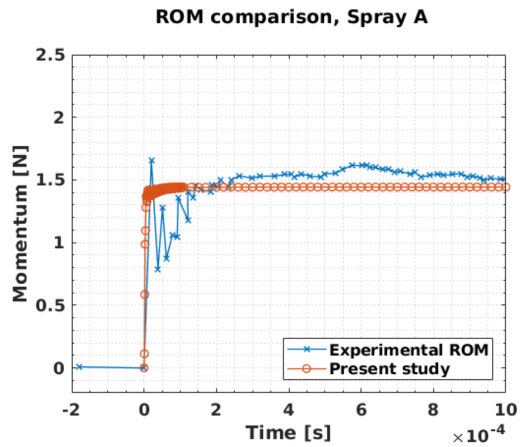

(c) Rate of momentum

Figure 4: Mass flow and momentum comparison for Spray A nozzle.

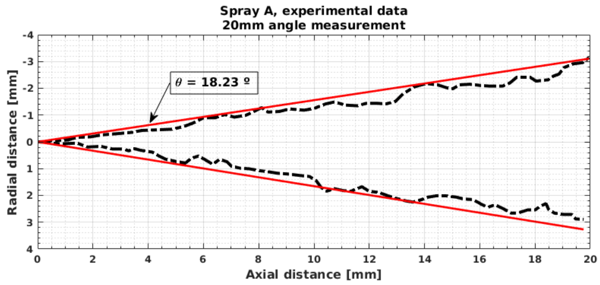

(a) Spray A, experimental angle (Pickett et al., 2013) contour and fitting lines. A DBI technique was used for measuring the angle at 22.3 kg/m^3 of discharge density and 150 MPa injection pressure.

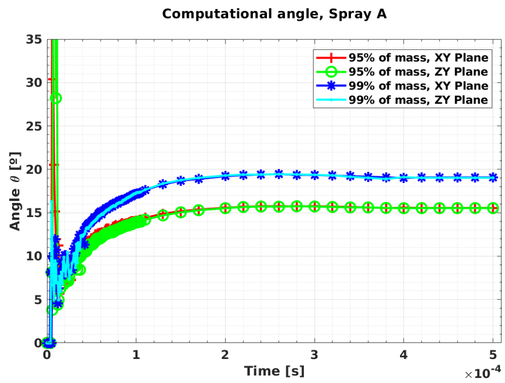

(b) Spray A, computational angle.

Figure 5: Spray A results.

the nozzle.

Taking into account the experimental data, an absolute error of 0.87° is found in the spray angle.

X-ray radiography technology applied to the study of the injection process (Duke et al., 2017; Kastengren et al., 2009, 2014, 2012) allows a deeper look inside the spray microscopic behaviour. Comparisons in projected mass density are provided below. Figure 6 shows several Gaussian profiles of projected mass density (PMD) along the spray axis (at 0.1 mm, 2 mm, 4 mm, 6 mm distance) on the XY plane. Although the Spray A injector is considered to be quasi-axi-symmetric, the slight deviation of the nozzle from the main injector body axis (Pickett et al., 2014) is captured by the deviation from 0 of the XY projection (Figure 6a, 6b, 6c, 6d). As reported in similar studies (Desantes et al., 2016b; Xue et al., 2015), even if the PMD is well captured along first millimetres of the spray, the CFD case shows higher values far from the nozzle exit. Beyond 6 mm, the decay of the projected mass density is severe, and the difference between experiments and simulation significantly grows. Similar conclusions can be obtained looking at 2-dimensional PMD contours available in Figures 7a and 7b. As it can be seen, the simulation provides a faster axial decay and a wider radial evolution of PMD compared to the experimental reference data as the spray develops far from the nozzle exit. Advanced turbulence approaches such as Large Eddy Simulation (LES), coupled with capturing interface methods, have shown to better describe the evolution of the projected mass density in literature studies, as reported in the literature (Anez et al., 2018; Desantes et al., 2017). However, since the main objective of the current study is to analyse the impact of the elliptical orifices on the nozzle flow behaviour and the primary atomization, the numerical setup used is deemed appropriate, since it has shown to be capable to properly capture the spray behaviour in the first millimetres of the nozzle outlet at a reduced computational cost.

Finally, a self similarity study for the velocity distribution has been performed. Figure 8 shows the evolution of the inverse of the velocity in the spray axis divided by the velocity at the nozzle orifice outlet. Additionally, the axial position has been made non-dimensional with respect to the nozzle equivalent diameter. As it can be seen, there is a linear increase after the so called intact length, as it would be predicted by gas jet theory. The results have an almost perfect match with the same information extracted from the work by Taub et al. (2013) based on Direct Numerical Simulations. The slope of this increase has been computed by doing a linear fit to the data extracted from the simulations and compared with experimental data from Hussein et al. (1994), showing a difference of approximately 4%. Both results can be seen as a further validation of the capability of the current model to properly capture the physics related with the momentum exchange between the fuel spray and the environment.

The previously mentioned result is complemented with the analysis of the radial distribution of the non-dimensional velocity, depicted in Figure 9. For axial positions equal or further than 24 times the equivalent diameter, all the radial profiles expressed in terms of the ratio between radial and axial positions collapse into a single curve. This corresponds to the disperse region of the spray, whose behaviour can be predicted according to gas jet theory. Instead, for closer positions to the nozzle tip a slight variation of this profile can be observed.

Multi-hole reference cylindrical nozzle

The second part of the model validation is focused on the analysis of the internal flow under cavitating conditions. Here, the mentioned 3D geometry of a commercial 6 holes injector with cylindrical orifices, previously characterised experimentally from an hydraulic standpoint (Salvador et al., 2011), is used. All simulations are performed with the same physical models already described for the spray A case, and have been run until a steady state flow was reached. Since cavitation is expected, the HRM model has been incorporated to the model equations. In a preliminary step, a mesh independence study was completed using three different levels of refinement, with an increment of 2^n size ratio for the nozzle region, as established in Table 5. Additionally, the Adaptive Mesh Refinement (AMR) method is activated for subgrid velocity levels higher than 1 m/s and 0.1 of void fraction.

Mesh independence study			
Base size = 384 μm	**Refinement level n**		
Region	**L**	**M**	**H**
Nozzle	2	3	4
Nozzle wall (3 levels)	5	6	7
AMR velocity	3	4	5
AMR void fraction	4	5	6
Needle	2	3	3
Total elements	18247	85687	389148

Table 5: Mesh configuration for the six orifices nozzle.

Mass flow rate and vapour mass at the outlet have been selected as the reference parameters for analysing the grid convergence. Once a steady state value of the selected variables has been reached, the convergence of the mesh was checked as described in Roache (1994) and Salvador et al. (2018a). The small committed error between the results and the Richardson extrapolation (P_{rh} < 0.47%), and the very low grid convergence index (GCI) leads to conclude that these variables are located into the asymptotic zone of

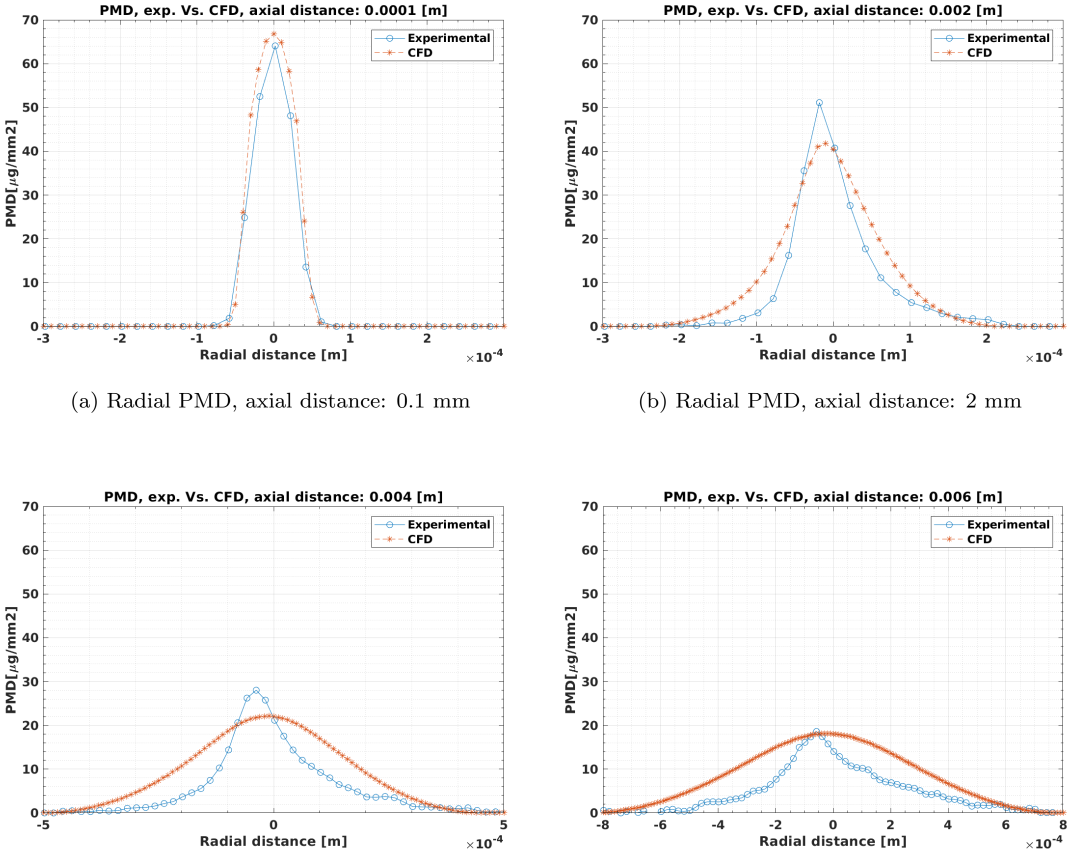

(a) Radial PMD, axial distance: 0.1 mm

(b) Radial PMD, axial distance: 2 mm

(c) Radial PMD, axial distance: 4 mm

(d) Radial PMD, axial distance: 6 mm

Figure 6: Projected mass density profiles on the XY plane, Spray A.

its mesh dependent curves with a mesh convergence order of 2. The GCI slightly varies between the low and medium mesh resolution (0.0021 and 0.0058 for mass flow and vapour mass, respectively) and the medium to high resolution step (0.0086 and 0.0012 for mass flow and vapour mass, respectively). It was then deemed valid due to the low values achieved. However, for the simulations ahead the configuration with the highest mesh refinement has been chosen for the internal flow. The decision was based on the importance of not only reproduce the mean value of the flow, but also the particular distribution of the velocity and vapour profiles at the nozzle outlet. Furthermore, the AMR performance can be greatly conditioned by the initial grid size as studied in Payri et al. (2019). A superior surface refinement ensures the stability of the calculations when cavitation appears, and the correct generation of a initial gradient for the AMR void fraction subgrid. It has to be noticed that for the nozzle with the highest eccentricity the resultant minor radius has 50 μm length. The cell size must take into account this reduction of the aspect ratio and provide a suitable number of elements inside the orifice.

The experimental validation of the flow was carried out by means of several mass flow rate measurements at three injection pressures and six back-pressures (Salvador et al., 2011). Figure 11 depicts the values for the CFD and experimental results. As appreciated, the code is able to properly reproduce the mass flow choking conditions (the point at which mass flow rate reaches a critical limit value). An error of 5.4% is found for the maximum injection pressure of 160 MPa. The error is expected to progressively decrease as the

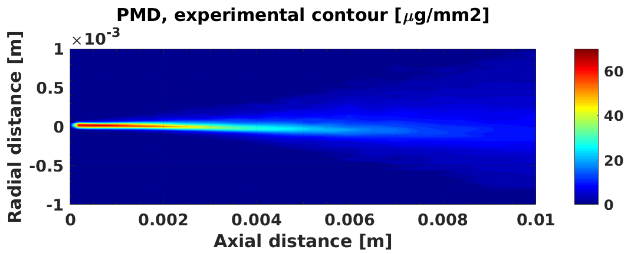

(a) Projected mass density in 2D view, X-Ray data from the Spray A.

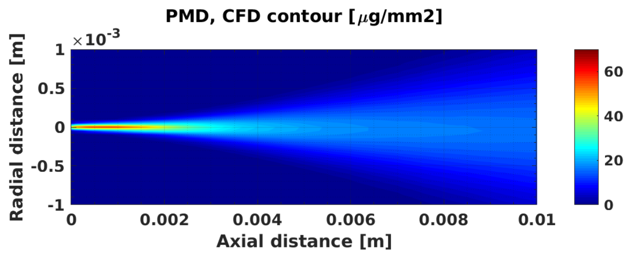

(b) Projected mass density in 2D view, CFD post-processed simulation from the Spray A.

Figure 7: Projected mass density contours, Spray A. Experimental data extracted from https://ecn.sandia.gov/rad675/ and reported in Kastengren et al. (2014)

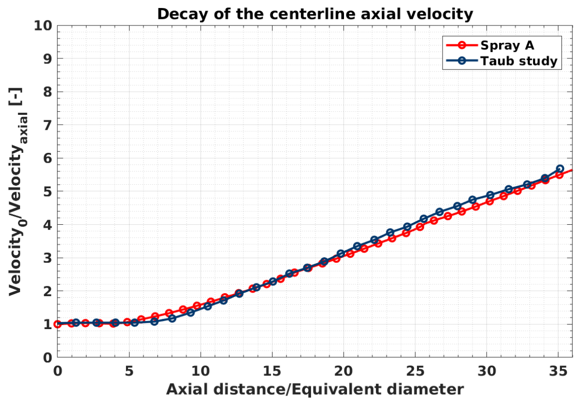

Figure 8: Axial evolution of the inverse of the non-dimensional velocity at the spray centerline.

injection pressure magnitude increases.

5. Results and discussion

A first sight to the effect of the eccentricity in the injection nozzle is carried out by the study of the inner flow. For this purpose, the main non-

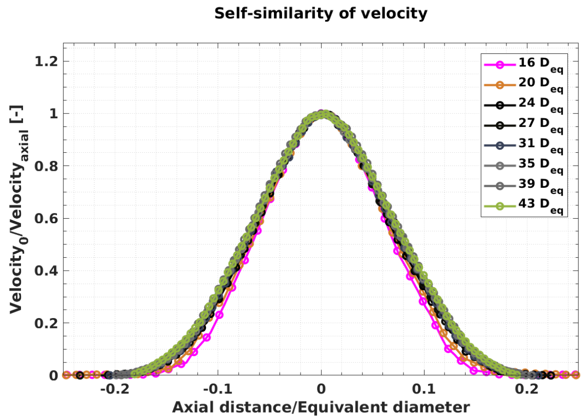

Figure 9: Radial distribution of the non-dimensional velocity

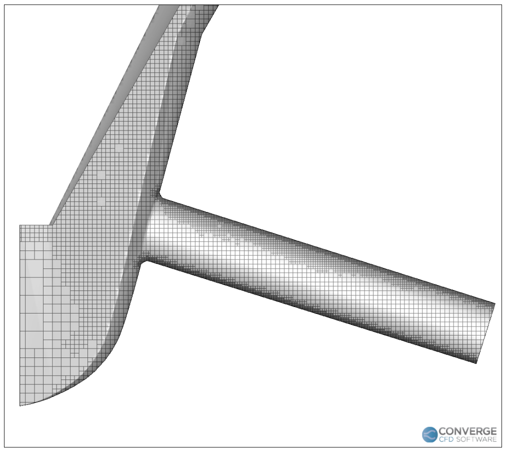

Figure 10: Detail of mesh configuration.

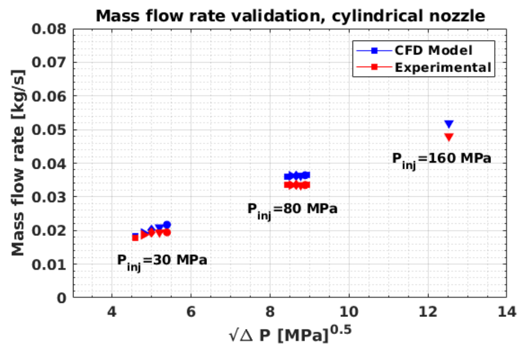

Figure 11: Experimental vs. Computational mass flow. Each symbol represents a different back pressure from 0.1 to 9 MPa.

dimensional flow coefficients of the nozzle, mainly including the discharge coefficient C_d, the velocity coefficient C_v and the area coefficient C_a, have been obtained (Salvador et al., 2015a). The discharge coefficient, C_d, has been calculated according to the ideal mass flow value based on Bernoulli's equation:

$$C_d = \frac{\dot{m_f}}{\rho_l A_0 u_{th}} = \frac{\dot{m_f}}{A_0\sqrt{2\rho_l \Delta P}} \quad , \tag{29}$$

where $\dot{m_f}$ is the mass flow, ρ_l is the liquid density, A_0 is the geometric outlet orifice area and ΔP is the pressure drop.

From the comparison of the nozzle effective vs. theoretical velocities, the velocity coefficient is calculated as:

$$C_v = \frac{u_{eff}}{u_{th}}. \tag{30}$$

Finally, the area coefficient can be calculated taking into account that the relationship $C_d = C_v C_a$.

Figure 12 shows the flow parameters from the elliptical nozzles calculations. As it can be seen, mass flow rate slightly rises its value as the eccentricity increases, while the momentum value remains almost unchanged. In the studies by Lee et al. (2006) and Ku et al. (2011), a similar behaviour was observed for the mass flow. It is also in agreement with a previous publication by the authors (Molina et al., 2014). The higher mass flow and similar outlet momentum are a consequence of a decreasing trend in the effective outlet velocity with increasing eccentricity, which can be explained by the interaction between the eccentricity and the intensity of cavitation. The internal flow parameters (Figure 12) show that cavitation is reduced as the eccentricity increases. Less cavitation produces a greater area coefficient, as it can be seen from the figure, but a lower velocity coefficient (Payri et al., 2005). In terms of mass flow, an increase would be foreseen when increasing the eccentricity, since the higher C_a would induce an also higher C_d if the velocity remained constant. However, since the velocity is also reduced when eccentricity diminishes, two opposing effects are found, preventing the mass flow rate and momentum from suffering major changes.

According to the literature, more intense cavitation field induces a slightly higher momentum (similar mass flow, higher velocity), which would enforce the spread angle and mixing process (Chaves et al., 1995; Payri et al., 2004a; Tamaki et al., 2001). Additionally, many previous works available in the literature (Hiroyasu and Miao, 2003; Naber and Siebers, 1996) show the spray penetration can be mostly linked to the spray momentum and spreading angle. Therefore, slightly larger spray penetration could be anticipated for the cylindrical nozzles, which are characterized by slightly larger momentum. However, the following paragraphs will demonstrate that the sole study of the average flow parameters at the nozzle outlet is not enough to account the influence of eccentricity in the spray performance.

First of all, not only the cavitation intensity but its distribution along the nozzle section needs to be considered. As it can be seen from Figure 13, although the intensity of the void fraction is higher in the nozzle with $e = 0.50$ (left side), the distribution of vapour in the most elliptical nozzle is wider over the whole section (right side). Even if the generation of vapour inside the nozzle is well known to improve the atomization from the literature, the low amount of experimental measurements from inside the nozzle hardens the complete understanding of how the vapour distribution itself affects the phenomena involved. As it could be anticipated, the aspect ratio of the elliptical nozzles (i.e. the ratio between major and minor radii) affects the vapour distribution field, in particular the interaction between the bottom and top side vapour in the nozzle outlet. Figures 13a and 13b show how the stream-lines are then approaching each other along the nozzle as eccentricity increases, which supports this effect. Hong et al. (2010) suggested that the cavitation should be improved in the cross sectional area of the elliptical nozzles because of a severe contraction of the stream-lines. However, this statement may not be applied to multi-hole configurations, since the stream-lines are not symmetric. Unlike single-hole nozzles, in the proposed geometries the vapour is generated mainly in the top-part of the cross-section. This section, where the fluid accelerates, is wider for the nozzles with higher aspect ratio, and allows a larger path for the most critical stream-lines. A larger local curvature distributes the stream flow and reduces the pressure drop, so the vapour peak is lower. Additionally, it enforces the distribution of the vapour over the whole section, as it was already seen in Figure 13. Furthermore, the higher perimeter of the ellipse provides a more significant interaction of the spray section with the chamber gas. With respect to the thermodynamic properties of the fluid, no major differences have been identified.

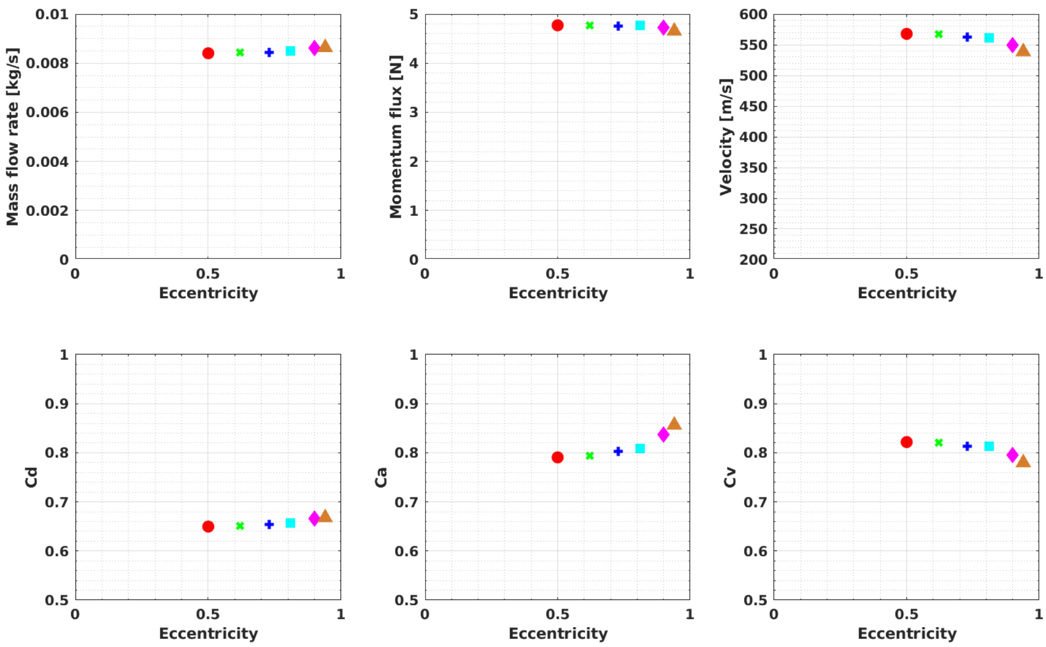

Figure 12: Hydraulic charaterization of the elliptical nozzles. The principal coefficients and variables have been calculated at the outlet for each nozzle. It includes the mass flow and momentum flux, effective velocity and non-dimensional parameters: the discharge coefficient, C_d, area coefficient, C_a, and velocity coefficient, C_v.

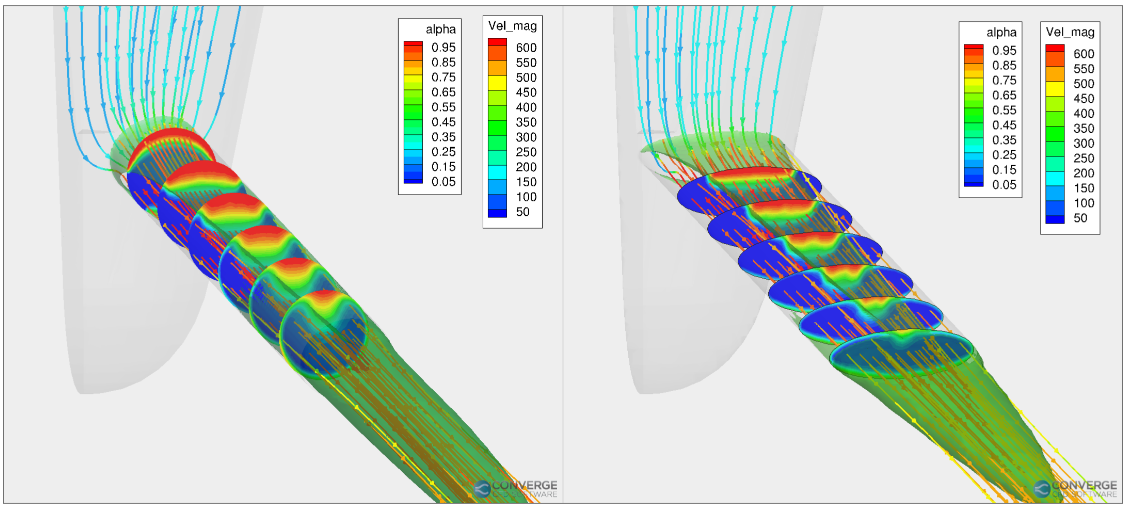

(a) Eccentricity = 0.50 (b) Eccentricity = 0.94

Figure 13: Flow conditions along the nozzle: the coloured stream-lines represent the variation of the velocity magnitude along the nozzle, while the radial slices show the void fraction evolution in six equally spaced sections. The iso-volume in green represents the void fraction for a value of 0.5. Notice how the vapour spreads further away from the orifice for the nozzle with lower eccentricity.

One important parameter that can be evaluated to start analysing the impact of the eccentricity in spray development is the evolution of the mixing field. This information is depicted in terms of the axial distribution of the fuel mass fraction (Figure 14), as well as the radial distribution of the fuel mass fraction at four axial positions and for two different planes (XY and ZY) in Figures 15a-15h. The axial distribution is defines in terms of the axial location divided by the equivalent diameter, defined as:

$$D_{eq} = D_o \sqrt{\frac{\rho_f}{\rho_a}} \tag{31}$$

where D_o is the diameter of a circle that would produce the same section as the outlet orifice of the eccentric nozzles, ρ_f the liquid fuel density and ρ_a the air density in the discharge chamber.

In the near nozzle region (up to 3 mm or 3.5 equivalent diameters), the axial evolution is very similar for all nozzles, while the radial distribution results are directly influenced by the nozzle morphology (Figure 15a and 15b). As the spray penetrates inside the chamber (3-8 mm, 3.5-9 equivalent diameters), the axial evolution is still similar, and the radial limits for the mass fraction start to become also more similar for both planes (Figure 15c and 15d). Beyond 8 mm (approximately 9 equivalent diameters), the axial evolution starts to be affected by the nozzle eccentricity, which can be also seen in the fact that the radial profiles associated to the more elliptical nozzles seem to reduce their fraction peak in favour of a wider curve (Figure 15e and 15f). A decreasing value of the liquid mass fraction peak can only take place if the equivalent quantity of liquid is radially scattered, that is, the angle of the spray is also bigger. An inversion of width between both XY and ZY planes (corresponding to the minor and major axis, respectively) appears before reaching the 12 mm (approximately 14 equivalent diameters) position. This phenomenon becomes more severe as the aspect ratio increases (Figures 15g and 15h). Similar behaviour has been found by Yu et al. (Yu et al., 2018) in cavitating single-hole nozzles. In that case, where the flow enters symmetrically (in the direction of the nozzle axis), the initial perturbation starts on the sides of the major axis due to a greater contraction of the stream-lines. This produces an initial larger dispersion in the ZY (major axis) plane (Hong et al., 2010). In the case of the present study, cavitation is generated in the top and bottom sections of the minor axis as a result of the inclination angle of the nozzle orifice with respect to the injector axis (Salvador et al., 2015a). Hence, a wider spreading angle would be expected for the XY plane.

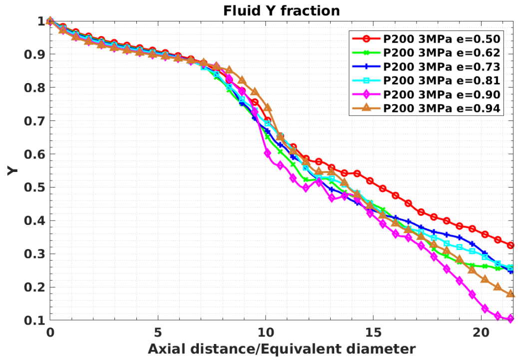

Figure 14: Axial liquid mass fraction

The radial and axial velocity profiles have also been extracted. The tendencies are similar to those of the liquid fuel mass fraction. A primary influence of the outlet geometry is followed by an almost perfect matching in the maximum value and shape of the velocity profiles as the spray develops in axial direction (Figures 16a, 16b, 16c, 16d). For an intermediate point (8 mm, 9 equivalent diameters), the velocity starts to decrease faster for higher eccentricity values (Figures 16e, 16f, 16g and 16h). A faster dispersion of the fuel over the chamber is consistent with an earlier velocity fall. The mass exchange between the injected liquid and the inert gas (because of turbulent friction) results in kinetic energy losses which are, in fact, velocity losses. A similar trend can be seen in Figure 17 looking at the evolution of the inverse of the centerline velocity divided by the outlet velocity. While in the case of a circular nozzle (i.e. symmetric jet) a linear trend would be seen, as it was already analyzed for Spray A data in Figure 8, for the elliptical geometries this linear trend can only be perceived for an axial distance up to 10 times the equivalent diameter. From that point on, inverse of the velocity clearly increases with a faster rate than a linear trend, actually more intense as the nozzle eccentricity increases.

Figure 18 represents the air entrainment for each nozzle spray. As it can be seen, there is a general trend of increasing entrainment as the eccentricity rises. A smooth growing trend is observed for the

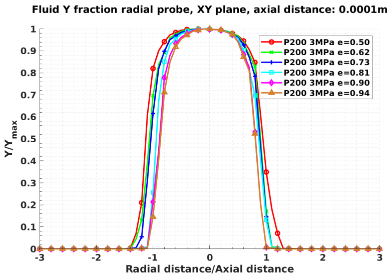

(a) XY, 0.1mm (0.12 D_{eq})

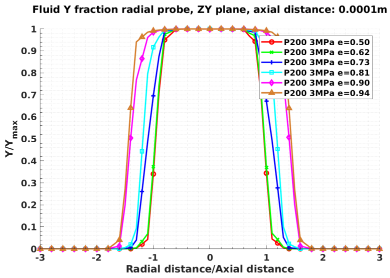

(b) ZY, 0.1mm (0.12 D_{eq})

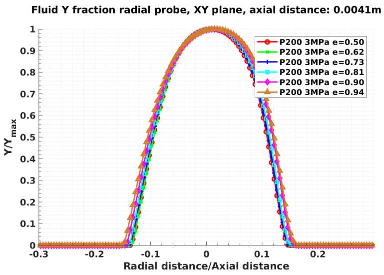

(c) XY, 4.1mm (4.86 D_{eq})

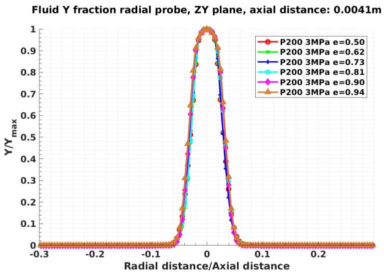

(d) ZY, 4.1mm (4.86 D_{eq})

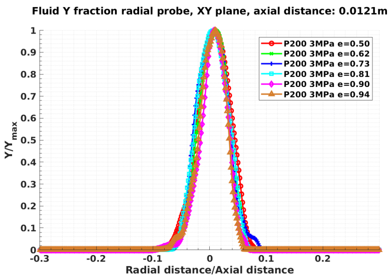

(e) XY, 12.1mm (14.37 D_{eq})

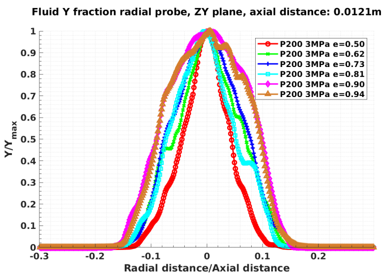

(f) ZY, 12.1mm (14.37 D_{eq})

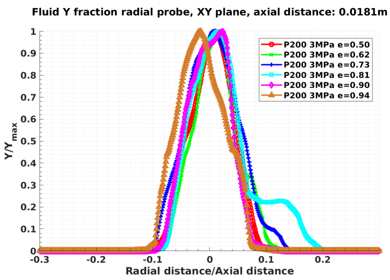

(g) XY, 18.1mm (21.5 D_{eq})

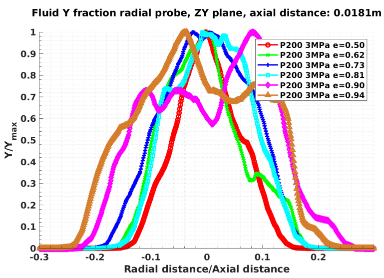

(h) ZY, 18.1mm (21.5 D_{eq})

Figure 15: Radial liquid mass fraction profiles for the elliptical nozzles.

first four nozzles ($e = 0.50 \div 0.81$) while the two last cases are characterised by a bigger initial entrainment. In line with the discussion above, the enhanced air entrainment is consistent with a wider divergence of the angle and a slightly bigger mass flow rate (Figure 12) (Araneo et al., 1999; MacGregor, 1991). Both liquid fuel mass fraction and velocity profiles indicate that the spreading angle in ZY plane is enhanced as the eccentricity of the nozzle increases. Taking this into account, its impact on the spray penetration can be evaluated. In this sense, if the spray momentum is defined as:

$$\dot{M}(x) = \dot{M}_0 = \dot{m}_f U_0 = \int_A \rho_f U^2(x) dA. \qquad (32)$$

The relationship between the spreading angle and the penetration can be established as follows (Desantes et al., 2006):

$$S(t) \propto M_f^{0.25} \rho_a^{-0.25} tan^{-0.5}(\theta/2) t^{0.5}. \qquad (33)$$

The penetration is then proportional to the momentum and inversely proportional to the tangent of the spreading angle. From Figure 14, it can be observed how beyond a medium distance from the nozzle outlet, the elliptical nozzles diminish the liquid fraction faster along the injection axis, which must be supported by an increment of the spreading angle. Given that the momentum (12) does not change significantly, an angle reduction will cause a slower penetration slope. From a qualitative view, Figure 19 shows how the 0.01 mass fraction isovolume regions for the most extreme nozzles (almost cylindrical and very elliptical), highlighting the wider dispersion from the most eccentric nozzle as the spray develops.

Even if the momentum value is nearly the same for all nozzles, the interaction of this momentum with the ambient gas is not. On the one hand, the surface of elliptical nozzles adds an extra perimeter of contact with the air for a same geometric area value. On the other hand, the momentum thickness (Krothapalli et al., 1981) varies across the section in different ways for all cases so a lineal behaviour is not necessarily expected between the sprays. This surface interaction gain between the discharge gas and the diesel jet is exponentially increasing with eccentricity. From Figure 20, the numerical breach in the shape area interaction between the first four nozzles ($e = 0.50 \div 0.81$) and the two last nozzles ($e = 0.90$ and 0.94) can provide some explanation to the leap in entrainment. The resulting jet shape at the outlet for the maximum accounted eccentricity originates a value of 21.27% over the initial cylindrical nozzle perimeter for the same geometric area. This fact makes the rise in surface interaction compatible in general terms with the results for the entrainment and angle.

Finally, Figures 21a and 21b show the average computed angle (section 3) for all the elliptical nozzles. The angle projected on XY plane (21a) oscillates around 14° with no clear trend. The deviation from the mean value (dotted grey line) does not exceed 1.5°. From what was exposed in the internal flow parameters, the more cylindrical nozzle should develop a higher XY angle due to a more intense cavitation. However, the decreasing thickness in that plane for the elliptical nozzles also favours the increment of the angle due to instabilities. These effects oppose each other and may be the cause of an almost constant XY angle. This behaviour can be also connected to the fluctuations produced by cavitation, given that it takes place in the top and bottom parts of the nozzle section (minor axis view, XY plane).

The pulsatile and unsteady instabilities of vapour could lead to a still transient deposition of liquid in the XY plane for the simulated time. Nevertheless, this result is in agreement with the mass fraction profiles in the radial XY plane (Figure 15e, 15g), where the limit threshold value of the mass fraction appears in almost the same radial coordinate. Differently, the angle on ZY projection depicted in Figure 21b shows a clear tendency also according to the right column of picture 15, indicating that the divergence of the angle in ZY is proportional to the eccentricity value. Continuing with the pattern previously suggested in the entrainment discussion, a smooth jump in the angle is found until a eccentricity value of 0.81 while the last two nozzles shows a wider but closer angle. Regarding the angle proximity between nozzles 5 and 6, the proposed simulations may have reached the eccentricity threshold value at which the spray angle no longer increases. An increment about 10° is detected for the maximum eccentricity nozzle with respect to the lower one. Hong et al. (2010) showed in its experiments with transparent nozzles how the angle increases in both major and minor axis planes when elliptical single-hole nozzles are subjected to cavitation. However, in those proposed geometries, the cavitation and hence the source of instabilities were located in the major axis extremes, the opposite to

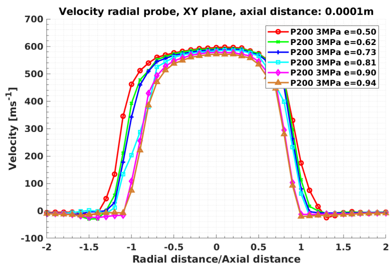

(a) XY, 0.1 mm (0.12 D_{eq})

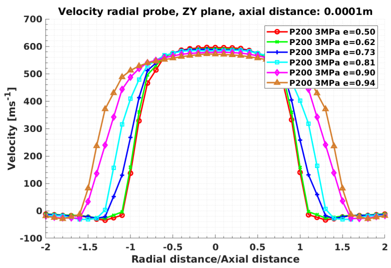

(b) ZY, 0.1 mm (0.12 D_{eq})

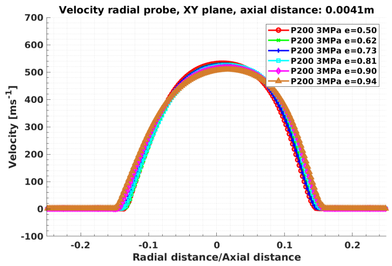

(c) XY, 4.1 mm (4.86 D_{eq})

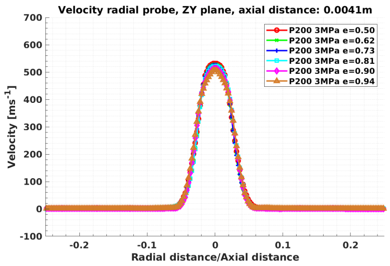

(d) ZY, 4.1 mm (4.86 D_{eq})

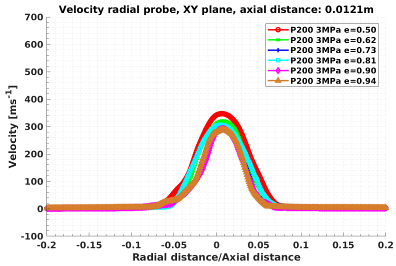

(e) XY, 12.1 mm (14.37 D_{eq})

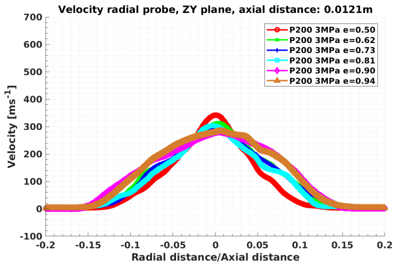

(f) ZY, 12.1 mm (14.37 D_{eq})

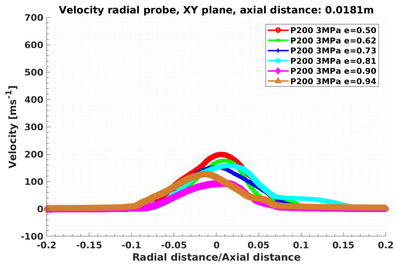

(g) XY, 18.1 (21.5 D_{eq}) mm

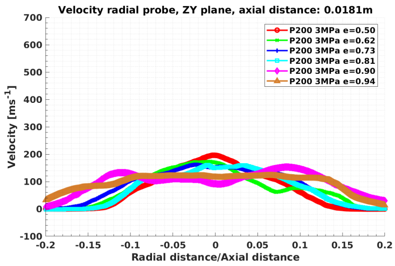

(h) ZY, 18.1 (21.5 D_{eq}) mm

Figure 16: Radial velocity profiles for the elliptical nozzles.

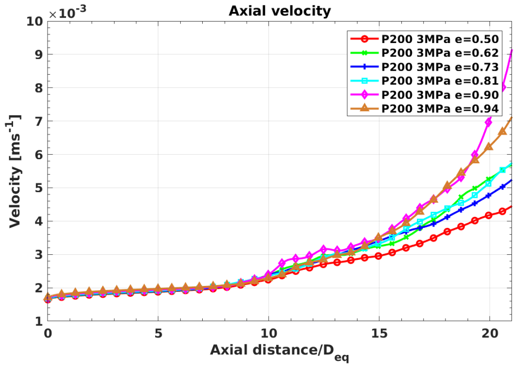

Figure 17: Axial liquid velocity

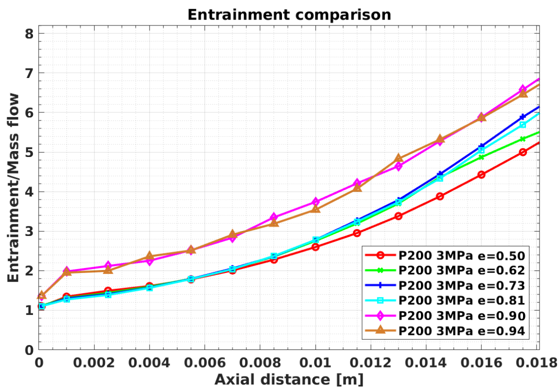

Figure 18: Jet entrainment.

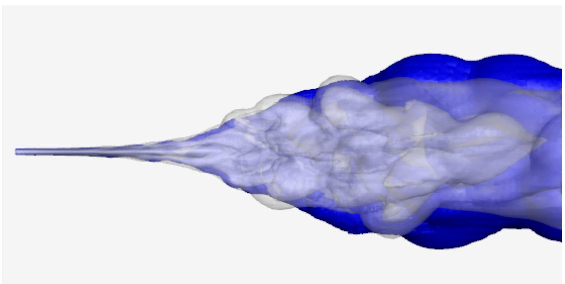

Figure 19: Iso-volume for a liquid mass fraction value of 0.01, ZY visualization plane. The nozzle of 0.50 eccentricity is depicted in white, the nozzle of 0.94 in blue.

that of the diesel nozzle of the present paper (Figure 13). As exposed by Ku et al. (2011), this fact produces a greater spreading angle in the major axis (ZY plane).

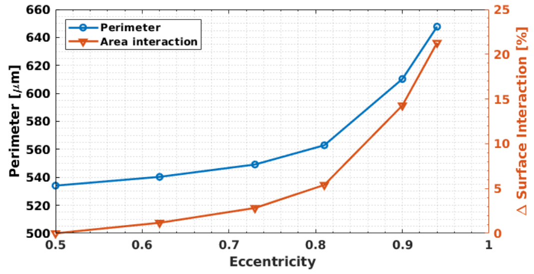

Figure 20: Geometrical effects of eccentricity over the spray interaction.

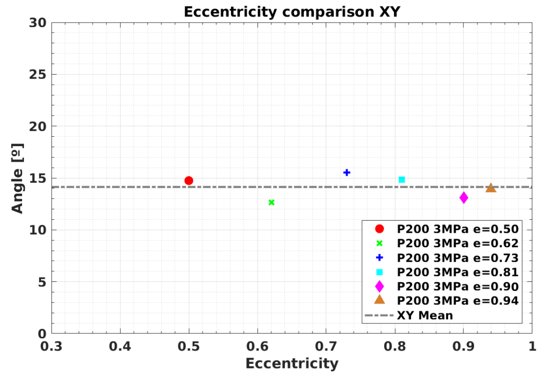

(a) Mean angle comparison in the minor axis plane (XY).

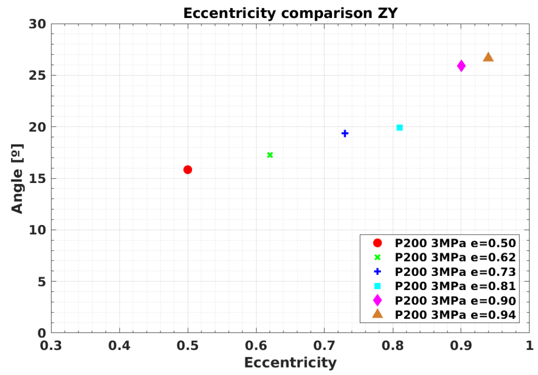

(b) Mean angle comparison in the major axis plane (ZY).

Figure 21: Angle comparison, elliptical nozzles.

Figure 22a depicts the temporal evolution of the angle for the nozzle simulation with highest aspect ratio ($e = 0.94$). A first view on the right side of Figure 5 shows an almost constant angle for the first millimetres of the spray up to 8 mm. At this point, the angle starts to grow and the trend is more significant. It is coherent with the absence of higher disturbances at the nozzle outlet on the ex-

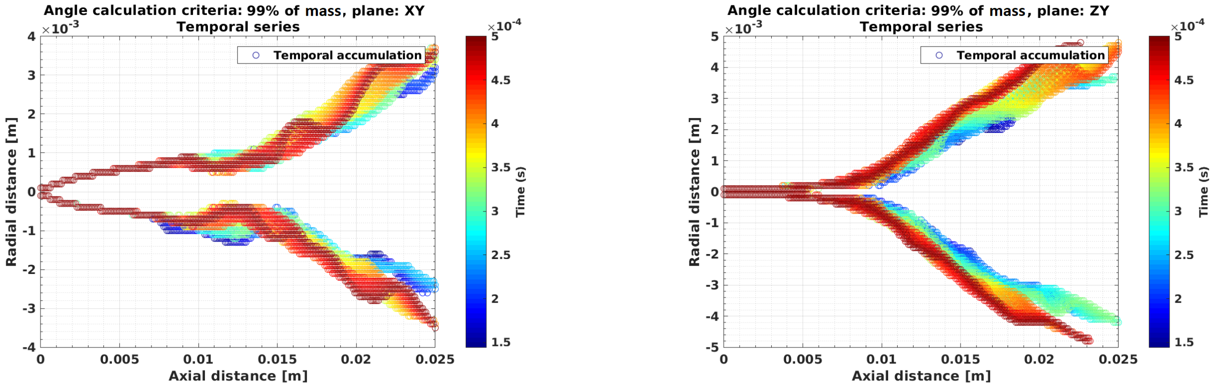

(a) Plane XY, minor axis

(b) Plane ZY, major axis

Figure 22: Temporal variation of angle, eccentricity = 0.94.

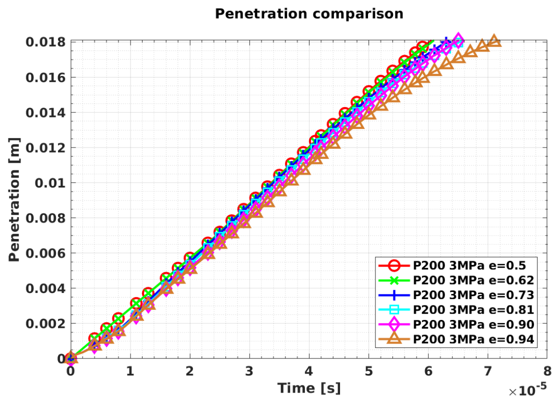

Figure 23: Penetration curves for the elliptical nozzles at full needle lift.

tremes of the major axis, unlike Kun et al. Image 22a traces a complete different behaviour from the computational angle. The minor axis plane (XY) angle strongly grows first millimetres of the spray. This issue is explained by the high disturbances at the outlet in the XY plane according to the existence of cavitation. Beyond 8 mm the XY angle suddenly reduces its growth. It can be seen how both XY and ZY angles share the inflexion point at which its width trends switch. As previously commented, the XY plane is expected to have a wider angle. For cylindrical nozzles, the spreading of fuel is enforced by cavitation generating a almost axi-symmetric and wider spray that non cavitating cylindrical nozzles. In related studies (Ho and Gutmark, 1987; Husain and Hussain, 1991; Hussain and Husain, 1989; Krothapalli et al., 1981), a switching axes behaviour has been repeatedly detected. In these works, the anomaly in the spray behaviour compared to cylindrical nozzles was attributed to a self-induced vortex of the elliptical spray. One similar behaviour was described by Yu et al. (2018) in experiments with single-hole nozzles. Although the bibliography above has only exposed single-hole nozzles, and it can not be directly compare to those of this study, several of its physical phenomena can be extrapolated to the performance of multi-hole nozzles. Figure 24 depicts the switching axis behaviour, first frames 24a, 24b, 24c and 24c shows the initial greater opening of the angle in the minor axis due to the effect of cavitation, the minor axis becomes the major axis. From frames 24d to 24i the instabilities start to rise in the new minor axis and it breaks in an inflexion point. The switching axis occurs between 24j and 24l. In picture 24m to 24t the greater dispersion in the ZY plane (geometrical major axis) starts to form a new and more defined elliptical shape. Summarizing, the general angle grows as the eccentricity rises being this fact more noticeable in the ZY angle (major axis) while in the minor XY axis the angle is at least as much bigger as the more cylindrical one.

A final outline over the problem commands the exam of penetration. Even if the simulations have been accomplished with a full needle lift, differences supporting the earlier discussion can be observed. Figure 23 provides the temporal evolution of penetration for all cases. As expected, a wider angle (high eccentricity values) generates a slower penetration curve (Desantes et al., 2006; Gimeno et al., 2016). However, it is true that in terms of pene-

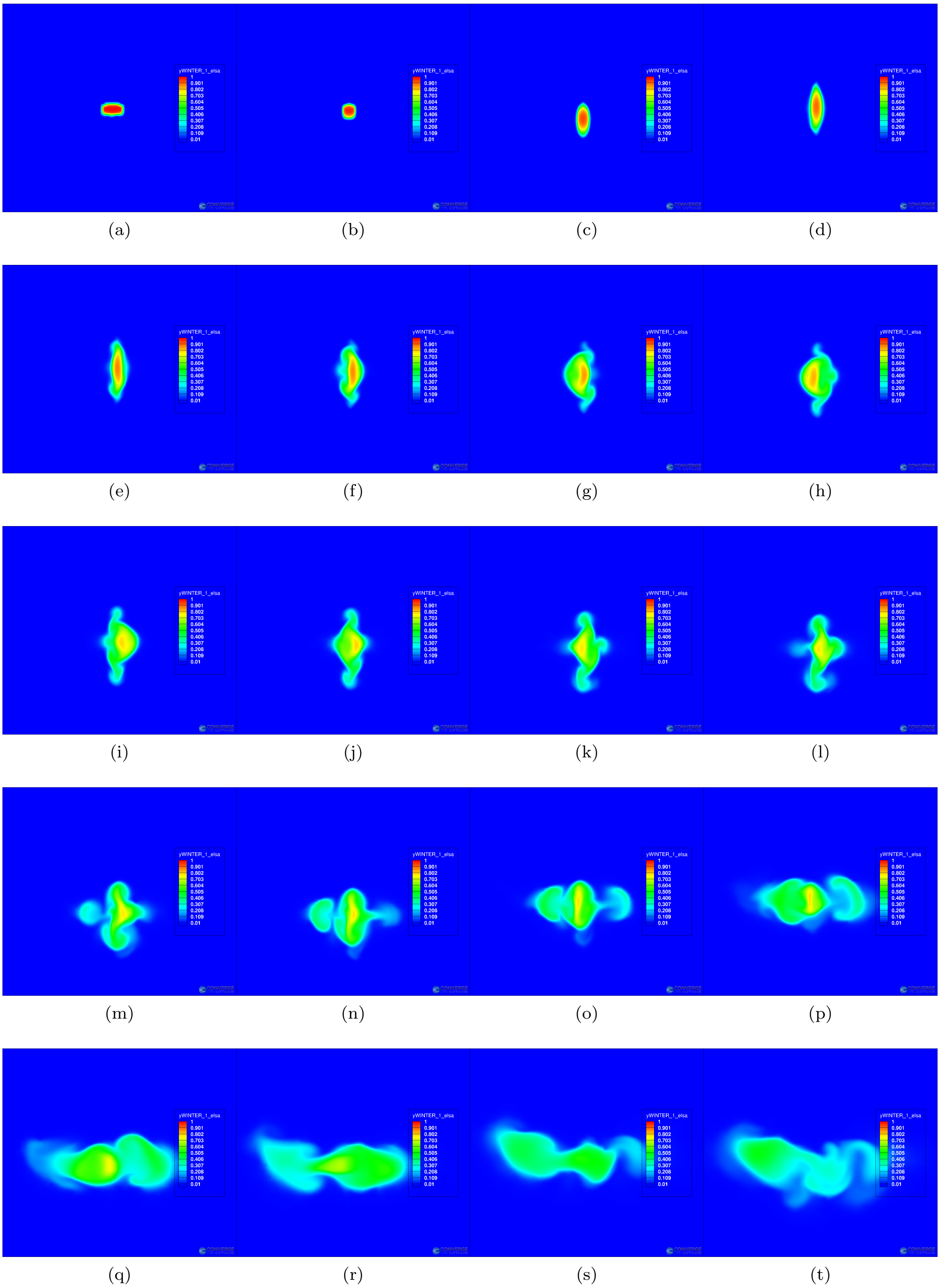

Figure 24: Main injection axis rotation due to self-induced vorticity of the jet, CFD.

tration, the difference between the nozzle 4 and 6 is not as big as it could be suggested by previous data. The evolution of the jet further from this point is an interesting topic, specially for big engines. Unfortunately, computational resources have limited the simulation space and the injection duration. For future works, larger time injections in order to clarify both angles behaviours must be carried out for a better understanding of this kind of nozzles. Even so, it has been demonstrated that the general influence of eccentricity enforces the spray atomization by means of a wider angle. Also, it has been discussed how the internal parameters such as momentum and mass flow, are not enough for fully describing the spray atomization potential and how the entrainment and fluid fraction along the spray are in resonance with the angle and entrainment. The increment of the surface area of jet-air interaction and the momentum thickness must be considered along with the self behaviour of the generated spray for the correct understanding of elliptical jets. A more complex model such as LES or near field DNS simulations could provide more specific data to measure these parameters.

6. Conclusions

Several elliptical nozzles with the same outlet area and different eccentricity have been simulated coupling the inner nozzle flow and spray formation by means of an advanced CFD code. The code has been previously validated in terms of the nozzle hydraulic performance and spray formation for both a single-hole conical nozzle as well as a multi-hole cylindrical one. In the case of the latest, the simulation included the activation of a HRM model, which accurately predicted the mass flow collapse induced by cavitation. This multi-hole geometry has been taking as a reference to produce the elliptical geometries.

The main conclusions of the study are summarized below:

1. A new study showing in depth the capabilities of elliptical nozzles in order to improve the atomization and mixing processes has been carried out by means of a numerical CFD model coupling the internal nozzle morphology and the external spray performance.

2. The $\Sigma - Y$ model is able to capture the internal geometric morphology of the nozzle and translate its characteristics to the spray.

3. For an equal area and boundary conditions, increasing the eccentricity for horizontal elliptical nozzles improves the discharge and area coefficients due to lower cavitation. The velocity coefficient is slightly decreased, producing very similar outlet momentum. In terms of cavitation, such geometries induce a vapour field with lower intensity but more dispersed across the outlet section of the orifice.

4. The spray behaviour has shown to be sensitive to the nozzle flow characteristics. In this sense, the spray cannot be fully understood only by simple average parameters at the nozzle outlet, which are the ones normally achievable with experimental tools. The way the nozzle shape interacts with the discharge chamber is critical.

5. In terms of spray characteristics, more elliptical nozzles produce an improvement of air entrainment, with the minor angle showing small variations, while the major angle increases significantly. Consequently, spray penetration tends to be reduced.

6. A significant increment of the angle and jet entrainment as the eccentricity rises are an indication that elliptical nozzles can help to improve the spray atomization processes.

Some of the aforementioned features found have been also confronted with previous literature works, providing consistent tends.

Declaration of conflicting interests

The author(s) declared no potential conflicts of interest with respect to the research, authorship, and/or publication of this article.

Acknowledgements

The authors would like to thank the computer resources, technical expertise and assistance provided by Universitat Politècnica de València in the use of the super-computer "Rigel". The authors want to express their gratitude to CONVERGENT SCIENCE Inc. and Convergent Science GmbH for their kind support for the CFD calculations with the CONVERGE software.

Funding

The author(s) disclosed receipt of the following financial support for the research, authorship, and/or publication of this article: This work was supported by the Ministerio de Ciencia, Innovación y Universidades of the Spanish Government. The PhD studies by Enrique C. Martínez-Miracle have been funded by the Agencia Estatal de Investigación of the Spanish Government and the ESF (European Social Fund), project "Desarrollo de modelos de combustión y emisiones HPC para el análisis de plantas propulsivas de transporte sostenibles" (TRA2017-89139-C2-1-R) by means of the "Subprograma Estatal de Formación del Programa Estatal de Promoción del Talento y su Empleabilidad en I+D+i".

References

Anez, J., Ahmed, A., Hecht, N., Duret, B., Reveillon, J., Demoulin, F.X., 2018. "Eulerian–Lagrangian spray atomization model coupled with interface capturing method for diesel injectors". International Journal of Multiphase Flow 113, 325–342. URL: https://doi.org/10.1016/j.ijmultiphaseflow.2018.10.009, doi:10.1016/j.ijmultiphaseflow.2018.10.009.

Arai, M., 2012. "Physics behind Diesel Sprays". ICLASS 2012, 12th Triennial International Conference on Liquid Atomization and Spray Systems, Heidelberg, Germany, September 2-6, 2012 Physics , 1–18URL: http://scholar.google.com/scholar?hl=en{&}btnG=Search{&}q=intitle:Physics+behind+Diesel+Sprays{#}0.

Araneo, L., Coghe, A., Brunello, G., Cossali, G.E., 1999. "Experimental investigation of gas density effects on diesel spray penetration and entrainment". SAE Technical Papers doi:10.4271/1999-01-0525.

Arcoumanis, C., Flora, H., Gavaises, M., Badami, M., 2000. "cavitation in real-size multi-hole diesel injector nozzles. SAE International URL: https://doi.org/10.4271/2000-01-1249, doi:https://doi.org/10.4271/2000-01-1249.

Battistoni, M., Duke, D.J., Swantek, A.B., Tilocco, F.Z., Powell, C.F., Som, S., 2015. Effects of noncondensable gas on cavitating nozzles. Atomization and Sprays 25, 453–483. URL: http://www.dl.begellhouse.com/journals/6a7c7e10642258cc,0ee7cd7c147d9638,3df6bd5d1c9936f1.html, doi:10.1615/AtomizSpr.2015011076.

Bilicki, E.W., Ali, S., Machinery, F.F., Academy, P., 1996. "Evaluation of the relaxation time of heat and mass exchange in the liquid-vapour bubble flow" 39.

Bilicki, Z., Kestin, J., 1990. "Physical Aspects of the Relaxation Model in Two-Phase Flow". Proceedings of the Royal Society A: Mathematical, Physical and Engineering Sciences 428, 379–397. URL: http://dx.doi.org/10.1098/rspa.1990.0040http://rspa.royalsocietypublishing.org/cgi/doi/10.1098/rspa.1990.0040, doi:10.1098/rspa.1990.0040.

Brusiani, F., Negro, S., Bianchi, G.M., Moulai, M., Neroorkar, K., Schmidt, D., 2013. "Comparison of the Homogeneous Relaxation Model and a Rayleigh Plesset Cavitation Model in Predicting the Cavitating Flow Through Various Injector Hole Shapes". SAE International URL: http://papers.sae.org/2013-01-1613/, doi:10.4271/2013-01-1613.

Chaves, H., Knapp, M., Kubitzek, A., Obermeier, F., Schneider, T., 1995. "Experimental study of cavitation in the nozzle hole of diesel injectors using transparent nozzles". SAE Technical Papers doi:10.4271/950290.

Dally, B.B., Fletcher, D.F., Masri, A.R., 1998. "Flow and mixing fields of turbulent bluff-body jets and flames". Combustion Theory and Modelling 2, 193–219. doi:10.1088/1364-7830/2/2/006.

David C.Wilcox, 1994. Turbulence Modelling CFD Wilcox.

Dechoz, J., Rozé, C., 2004. Surface tension measurement of fuels and alkanes at high pressure under different atmospheres. Applied Surface Science 229, 175–182. URL: http://www.sciencedirect.com/science/article/pii/S016943320400090X, doi:10.1016/j.apsusc.2004.01.057.

Desantes, J.M., Garcia-Oliver, J., Pastor, J., Pandal, A., Naud, B., Matusik, K., Duke, D., Kastengren, A., Powell, C., Schmidt, D., 2017. "Modelling and validation of near-field Diesel spray CFD simulations based on the Σ -Y model", in: ILASS 2017. URL: https://www.cmt.upv.es/ILASS2017/Default.aspx, doi:10.4995/ILASS2017.2017.4715.

Desantes, J.M., García-Oliver, J.M., García, A., Xuan, T., 2018. "Optical study on characteristics of non-reacting and reacting diesel spray with different strategies of split injection". International Journal of Engine Research URL: http://journals.sagepub.com/doi/10.1177/1468087418773012, doi:10.1177/1468087418773012.

Desantes, J.M., Garcia-Oliver, J.M., Pastor, J.M., Pandal, A., Baldwin, E., Schmidt, D.P., 2016a. "Coupled/decoupled spray simulation comparison of the ECN spray a condition with the Σ-Y Eulerian atomization model". International Journal of Multiphase Flow 80, 89–99. doi:10.1016/j.ijmultiphaseflow.2015.12.002.

Desantes, J.M., Garcia-Oliver, J.M., Pastor, J.M., Pandal, A., Baldwin, E., Schmidt, D.P., 2016b. "Coupled/decoupled spray simulation comparison of the ECN spray a condition with the Σ-Y Eulerian atomization model". International Journal of Multiphase Flow 80, 89–99. doi:10.1016/j.ijmultiphaseflow.2015.12.002.

Desantes, J.M., Payri, R., Salvador, F.J., Gil, A., 2006. "Development and validation of a theoretical model for diesel spray penetration". Fuel 85, 910–917. URL: http://www.sciencedirect.com/science/article/pii/S0016236105004084.

Desantes, J.M., Salvador, F.J., Carreres, M., Jaramillo, D., 2015. "Experimental Characterization of the Thermodynamic Properties of Diesel Fuels Over a Wide Range of Pressures and Temperatures". SAE International Journal of Fuels and Lubricants 8, 951–2015. URL: http://papers.sae.org/2015-01-0951/, doi:10.4271/2015-01-0951.

Desantes, J.M., Salvador, F.J., Lopez, J.J., De la Morena, J., 2011. "Study of mass and momentum transfer in diesel sprays based on X-ray mass distribution measurements and on a theoretical derivation". Experiments in Fluids 50, 233–246. URL: http://link.springer.com/article/10.1007/s00348-010-0919-8, doi:10.1007/s00348-010-0919-8.

Desjardins, O., Pitsch, H., 2010. "Detailed Numerical Investigation of Turbulent Atomization of Liquid Jets". Atomization and Sprays 20, 311–336. doi:10.1615/AtomizSpr.v20.i4.40.

Downar-Zapolski, P., Bilicki, Z., Bolle, L., Franco, J., 1996. "The non-equilibrium relaxation model for one-dimensional flashing liquid flow". International Journal of Multiphase Flow 22, 473–483. doi:10.1016/0301-9322(95)00078-X.

Duke, D.J., Matusik, K.E., Kastengren, A.L., Swantek, A.B., Sovis, N., Payri, R., Viera, J.P., Powell, C.F., 2017. "X-ray radiography of cavitation in a beryllium alloy nozzle". International Journal of Engine Research 18, 39–50. doi:10.1177/1468087416685965.

Dumouchel, C., 2008. On the experimental investigation on primary atomization of liquid streams. Experiments in Fluids 45, 371–422. URL: http://link.springer.com/article/10.1007/s00348-008-0526-0, doi:10.1007/s00348-008-0526-0.

Espey, C., Dec, J.E., Litzinger, T.A., Santavicca, D.A., 1997. "Planar laser rayleigh scattering for quantitative vapor-fuel imaging in a diesel jet". Combustion and Flame 109, 65–86. URL: http://www.sciencedirect.com/science/article/pii/S0010218096001265, doi:10.1016/S0010-2180(96)00126-5.

Garcia-Oliver, J.M., Pastor, J.M., Pandal, A., Trask, N., Baldwin, E., Schmidt, D.P., 2013. "Diesel Spray Cfd Simulations Based on the Σ-Υ Eulerian Atomization Model". Atomization and Sprays 23, 71–95. URL: http://www.begellhouse.com/journals/6a7c7e10642258cc,720d793326544e5b,3c72926a063b38a0.html, doi:10.1615/AtomizSpr.2013007198.

Gimeno, J., Bracho, G., Martí-Aldaraví, P., Peraza, J.E., 2016. "Experimental study of the injection conditions influence over n-dodecane and diesel sprays with two ECN single-hole nozzles. Part I: Inert atmosphere". Energy Conversion and Management 126, 1146–1156. URL: http://dx.doi.org/10.1016/j.enconman.2016.07.077, doi:10.1016/j.enconman.2016.07.077.

He, Z., Zhang, L., Saha, K., Som, S., Duan, L., Wang, Q., 2017. Investigations of effect of phase change mass transfer rate on cavitation process with homogeneous relaxation model. International Communications in Heat and Mass Transfer 89, 98–107. URL: https://doi.org/10.1016/j.icheatmasstransfer.2017.09.021, doi:10.1016/j.icheatmasstransfer.2017.09.021.

Heywood, J.B., 1988. "Internal combustion engine fundamentals". McGraw-Hill.

Hiroyasu, H., 2000. " Spray Breakup Mechanism from the Hole-type Nozzle and its Applications ". Automization and Sprays: Journal of the International Institutions for Liquid Atomization and Spray Systems 10, 511–527. doi:10.1615/AtomizSpr.v10.i3-5.130.

Hiroyasu, H., Arai, M., 1990. "Structures of Fuel Sprays in Diesel Engines" 2002. URL: https://www.sae.org/content/900475/, doi:10.4271/900475.

Hiroyasu, H., Kadota, T., 1974. "Fuel droplet size distribution in diesel combustion chamber". SAE International doi:https://doi.org/10.4271/740715.

Hiroyasu, H., Miao, H., 2003. "Measurement and Calculation of Diesel Spray Penetration". Proceedings of ICLASS Conference URL: http://www.ilasseurope.org/ICLASS/iclass2003/fullpapers/1413.pdf.

Ho, C.M., Gutmark, E., 1987. "Vortex induction and mass entrainment in a small-aspect-ratio elliptic jet". Journal of Fluid Mechanics 179, 383. URL: http://www.journals.cambridge.org/abstract{_}S0022112087001587, doi:10.1017/S0022112087001587.

Hong, J.G., Ku, K.W., Kim, S.R., Lee, C.W., 2010. "Effect of cavitation in circular nozzle and elliptical nozzles on the spray characteristic". Atomization and Sprays 20, 877–886. URL: http://www.scopus.com/inward/record.url?eid=2-s2.0-79955791257{&}partnerID=tZOtx3y1, doi:10.1615/AtomizSpr.v20.i10.40.

Hoyas, S., Gil, A., Margot, X., Khuong-Anh, D., Ravet, F., 2013. "Evaluation of the Eulerian-Lagrangian Spray Atomization (ELSA) model in spray simulations: 2D cases". Mathematical and Computer Modelling doi:10.1016/j.mcm.2011.11.006.

https://convergecfd.com, . Converge is a trade mark of convergent science.

Husain, H.S., Hussain, F., 1991. "Elliptic jets. part 2. dynamics of coherent structures: Pairing". Journal of Fluid Mechanics 233, 439–482. doi:10.1017/S0022112091000551.

Hussain, F., Husain, H.S., 1989. "Elliptic jets. Part 1. Characteristics of unexcited and excited jets". Journal of Fluid Mechanics 208, 257–320. URL: https://www.cambridge.org/core/product/identifier/S0022112089002843/type/journal{_}article, doi:10.1017/S0022112089002843.

Hussein, H.J., Capp, S.P., George, W.K., 1994. Velocity measurements in a high-Reynolds-number, momentum-conserving, axisymmetric, turbulent jet. Journal of Fluid Mechanics 258, 31–75.

Idicheria, C.A., Pickett, L.M., 2011. Ignition , soot formation , and end-of-combustion transients in diesel combustion under high-EGR conditions. International Journal of Engine Research 12, 1–17. doi:10.1177/1468087411399505.

Ishii, M., Hibiki, T., 2006. "Thermo-fluid dynamics of two-phase flow". Thermo-Fluid Dynamics of Two-Phase Flow , 1–462doi:10.1007/978-0-387-29187-1.

Janicka, J., Peters, N., 1982. "Prediction of turbulent jet diffusion flame lift-off using a pdf transport equation". Symposium (International) on Combustion 19, 367–374. doi:10.1016/S0082-0784(82)80208-7.

Kastengren, A., Powell, C.F., Liu, Z., Wang, J., 2009. "Time resolved, three dimensional mass distribution of diesel sprays measured with X-ray radiography". SAE Technical Papers doi:10.4271/2009-01-0840.

Kastengren, A.L., Tilocco, F.Z., Duke, D., Powell, C.F., Zhang, X., Moon, S., 2014. "Time-resolved X-ray radiography of sprays from Engine Combustion Network spray a diesel injectors". Atomization and Sprays 24, 251–272. doi:10.1615/AtomizSpr.2013008642.

Kastengren, A.L., Tilocco, F.Z., Powell, C.F., Manin, J., Pickett, L.M., Payri, R., Bazyn, T., 2012. "Engine Combustion Network (ECN): Measurements of Nozzle Geometry and Hydraulic Behavior". Atomization and Sprays 22, 1011–1052. doi:10.1615/AtomizSpr.2013006309.

Kolev, N.I., 2012. "Multiphase Flow Dynamics 4: Turbulence, Gas Adsorption and Release, Diesel Fuel Properties". Springer.

Krothapalli, A., Baganoff, D., Karamcheti, K., 1981. "On the mixing of a rectangular jet". Journal of Fluid Mechanics 107, 201–220. doi:10.1017/S0022112081001730.

Ku, K.W., Hong, J.G., Lee, C.W., 2011. "Effect of internal flow structure in circular and elliptical nozzles on spray characteristics". Atomization and Sprays 21, 655–672. doi:10.1615/AtomizSpr.2012004192.

Launder, B., Sharma, B., 1974. "Application of the energy-dissipation model of turbulence to the calculation of flow near a spinning disc". Letters in Heat and Mass Transfer 1, 131–137. URL: https://linkinghub.elsevier.com/retrieve/pii/0094454874901507, doi:10.1016/0094-4548(74)90150-7.

Launder, B.E., Spalding, D.B., 1974. "The numerical computation of turbulent flows". Computer Methods in Applied Mechanics and Engineering 3, 269–289. doi:10.1016/0045-7825(74)90029-2, arXiv:1204.1280v1.

Lebas, R., Menard, T., Beau, P., Berlemont, A., Demoulin, F.X., . "Numerical simulation of primary break-up and atomization: DNS and modelling study" 35, 247–260. URL: http://linkinghub.elsevier.com/retrieve/pii/S0301932208001821http://www.sciencedirect.com/science/article/pii/S0301932208001821, doi:10.1016/j.ijmultiphaseflow.2008.11.005.

Lee, C.w., Kim, I., Koo, K.w., Park, J., Lee, Y., 2006. "Experimental study of the effects of nozzle hole geometry for a DI diesel engine", in: ICLASS 2006, Kyoto.

Lefebvre, A., McDonell, V., 2017. "Atomization and Sprays, Second Edition.". URL: https://www.crcpress.com/Atomization-and-Sprays-Second-Edition/Lefebvre-McDonell/p/book/9781498736251, doi:10.1016/0009-2509(90)87140-N.

López, J.J., De La Garza, O.A., De La Morena, J., Martínez-Martínez, S., 2017. "Effects of cavitation in common-rail diesel nozzles on the mixing process". International Journal of Engine Research 18, 1017–1034. doi:10.1177/1468087417697759.

MacGregor, S.A., 1991. "Air entrainment in spray jets". International Journal of Heat and Fluid Flow 12, 279–283. doi:10.1016/0142-727X(91)90064-3.

Macian, V., Bermudez, V., Payri, R., Gimeno, J., 2003. "New Technique for Determination of Internal Geometry of a Diesel Nozzle With the Use of Silicone Methodology". Experimental Techniques 27, 39–43. URL: http://doi.wiley.com/10.1111/j.1747-1567.2003.tb00107.x, doi:10.1111/j.1747-1567.2003.tb00107.x.

Manin, J., Bardi, M., Pickett, L.M., Dahms, R.N., Oefelein, J.C., 2014. Microscopic investigation of the atomization and mixing processes of diesel sprays injected into high pressure and temperature environments. Fuel 134, 531–543. URL: http://dx.doi.org/10.1016/j.fuel.2014.05.060, doi:10.1016/j.fuel.2014.05.060.

Matsson, A., Andersson, S., 2002. "The effect of non-circular nozzle holes on combustion and emission formation in a heavy duty diesel engine". SAE Technical Papers doi:10.4271/2002-01-2671.

Molina, S., Salvador, F.J., Carreres, M., Jaramillo, D., 2014. "A computational investigation on the influence of the use of elliptical orifices on the inner nozzle flow and cavitation development in diesel injector nozzles". Energy Conversion and Management 79, 114–127. URL: http://dx.doi.org/10.1016/j.enconman.2013.12.015, doi:10.1016/j.enconman.2013.12.015.

Naber, J., Siebers, D.L., 1996. "Effects of Gas Density and Vaporization on Penetration and Dispersion of Diesel Sprays" , 960034URL: http://papers.sae.org/960034/, doi:10.4271/960034.

Pandal Blanco, A., 2016. "Implementation and Development of an Eulerian Spray Model for CFD simulations of diesel Sprays". Ph.D. thesis. Universitat Politècnica de València. Valencia (Spain). URL: https://riunet.upv.es/handle/10251/68490, doi:10.4995/Thesis/10251/68490.

Payri, F., Bermúdez, V., Payri, R., Salvador, F.J., 2004a. "The influence of cavitation on the internal flow and the spray characteristics in diesel injection nozzles". Fuel 83, 419–431. doi:10.1016/j.fuel.2003.09.010.

Payri, R., García, J.M., Salvador, F.J., Gimeno, J., 2005. "Using spray momentum flux measurements to understand the influence of diesel nozzle geometry on spray characteristics". Fuel 84, 551–561. doi:10.1016/j.fuel.2004.10.009.

Payri, R., Guardiola, C., Salvador, F., Gimeno, J., 2004b. "Critical Cavitation Number Determination in Diesel Injection Nozzles". Experimental Techniques 28, 49–52. URL: http://doi.wiley.com/10.1111/j.1747-1567.2004.tb00164.x, doi:10.1111/j.1747-1567.2004.tb00164.x.

Payri, R., Novella, R., Carreres, M., Belmar-Gil, M., 2019. "Study about the influence of an automatic meshing algorithm on numerical simulations of a gaseous-fueled Lean Direct Injection (LDI) gas turbine combustor in non-reactive conditions". URL: https://ilass19.sciencesconf.org/247299.

Payri, R., Salvador, F.J., Carreres, M., De La Morena, J., 2016. "Fuel temperature influence on the performance of a last generation common-rail diesel ballistic injector. Part II: 1D model development, validation and analysis". Energy Conversion and Management 114, 376–391. doi:10.1016/j.enconman.2016.02.043.

Payri, R., Salvador, J., Gimeno, J., De la Morena, J., 2011. "Analysis of Diesel Spray Atomization By Means of a Near-Nozzle Field Visualization Technique". Atomization and Sprays 21, 753–774. URL: http://www.dl.begellhouse.com/journals/6a7c7e10642258cc,3ca32fb40c63ad5e,65800d4d10472c6e.html, doi:10.1615/AtomizSpr.2012004051, arXiv:arXiv:1011.1669v3.

Pickett, L.M., Manin, J., Genzale, C.L., Siebers, D.L., Musculus, M.P., Idicheria, C.A., 2011. "Relationship Between Diesel Fuel Spray Vapor Penetration/Dispersion and Local Fuel Mixture Fraction". SAE International Journal of Engines 4, 764–799. doi:10.4271/2011-01-0686.

Pickett, L.M., Manin, J., Kastengren, A., Powell, C., 2014. "Comparison of Near-Field Structure and Growth of a Diesel Spray Using Light-Based Optical Microscopy and X-Ray Radiography". SAE International Journal of Engines 7, 1044–1053. doi:10.4271/2014-01-1412.

Pickett, L.M., Manin, J., Payri, R., Bardi, M., Gimeno, J., 2013. "Transient rate of injection effects on spray development". SAE Technical Papers 6, 15–16. doi:10.4271/2013-24-0001.

Pope, S.B., 1978. "An explanation of the turbulent round-jet/plane-jet anomaly". AIAA Journal 16, 279–281. doi:10.2514/3.7521.

Reitz, R., 1987. "modeling atomization processes in high-pressure vaporizing sprays". Atomisation Spray Technology 3, 309–337.

Reitz, R.D., Bracco, F.V., 1982. "Mechanism of atomization of a liquid jet". Physics of Fluids 25, 1730–1742. doi:10.1063/1.863650.

Reitz, R.D., Diwakar, R., 1987. "Structure of High-Pressure Fuel Sprays" URL: https://www.sae.org/content/870598/, doi:10.4271/870598.

Roache, P.J., 1994. "Perspective: A Method for Uniform Reporting of Grid Refinement Studies". Journal of Fluids Engineering 116, 405. URL: http://fluidsengineering.asmedigitalcollection.asme.org/article.aspx?articleid=1427780, doi:10.1115/1.2910291.

Salvador, F.J., Carreres, M., De la Morena, J., Martínez-Miracle, E., 2018a. "Computational assessment of temperature variations through calibrated orifices subjected to high pressure drops: Application to diesel injection nozzles". Energy Conversion and Management 171, 438–451. URL: https://linkinghub.elsevier.com/retrieve/pii/S0196890418305867, doi:10.1016/j.enconman.2018.05.102.

Salvador, F.J., Carreres, M., Jaramillo, D., Martínez-López, J., 2015a. "Analysis of the combined effect of hydrogrinding process and inclination angle on hydraulic performance of diesel injection nozzles". Energy Conversion and Management 105, 1352–1365. URL: http://dx.doi.org/10.1016/j.enconman.2015.08.035, doi:10.1016/j.enconman.2015.08.035.

Salvador, F.J., De la Morena, J., Bracho, G., Jaramillo, D., 2018b. "Computational investigation of diesel nozzle internal flow during the complete injection event". Journal of the Brazilian Society of Mechanical Sciences and Engineering 40. doi:10.1007/s40430-018-1074-z.

Salvador, F.J., Gimeno, J., Pastor, J.M., Martí-Aldaraví, P., 2014. "Effect of turbulence model and inlet boundary condition on the diesel spray behavior simulated by an eulerian spray atomization (ESA) model". International Journal of Multiphase Flow 65, 108–116. URL: http://dx.doi.org/10.1016/j.ijmultiphaseflow.2014.06.003, doi:10.1016/j.ijmultiphaseflow.2014.06.003.

Salvador, F.J., Hoyas, S., Novella, R., Martinez-Lopez, J., 2011. "Numerical simulation and extended validation of two-phase compressible flow in diesel injector nozzles". Proceedings of the Institution of Mechanical Engineers, Part D: Journal of Automobile Engineering 225, 545–563. doi:10.1177/09544070JAUTO1569.

Salvador, F.J., de la Morena, J., Carreres, M., Jaramillo, D., 2017. "Numerical analysis of flow characteristics in diesel injector nozzles with convergent-divergent orifices". Proceedings of the Institution of Mechanical Engineers, Part D: Journal of Automobile Engineering 231, 1935–1944. doi:10.1177/0954407017692220.

Salvador, F.J., Romero, J.V., Roselló, M.D., Jaramillo, D., 2015b. "Numerical simulation of primary atomization in diesel spray at low injection pressure". Journal of Computational and Applied Mathematics 291, 94–102. URL: http://linkinghub.elsevier.com/retrieve/pii/S0377042715001971http://dx.doi.org/10.1016/j.cam.2015.03.044, doi:10.1016/j.cam.2015.03.044.

Schmidt, D.P., 1997. "Cavitation in Diesel Fuel Injector Nozzles". Ph.D. thesis. University of Wisconsin - Madison. Wisconsin.

Schmidt, D.P., Gopalakrishnan, S., Jasak, H., 2010. "Multi-dimensional simulation of thermal non-equilibrium channel flow". International Journal of Multiphase Flow 36, 284–292. URL: http://linkinghub.elsevier.com/retrieve/pii/S030193220900192X, doi:10.1016/j.ijmultiphaseflow.2009.11.012.

Schulz, C., Sick, V., 2005. Tracer-LIF diagnostics: quantitative measurement of fuel concentration, temperature and fuel/air ratio in practical combustion systems. Progress in Energy and Combustion Science 31, 75–121. URL: http://linkinghub.elsevier.com/retrieve/pii/S0360128504000619, doi:10.1016/j.pecs.2004.08.002.

https://ecn.sandia.gov/ecn-data search/, . Engine Combustion Network data search. URL: https://ecn.sandia.gov/ecn-data-search/.

Senecal, K., Pomraning, E.D., Us, W.I., Jared, K., Horeb, M., Us, W.I., 2011. "Method and apparatus for automated grid formation in multi-cell system dynamics models".

Sforza, P.M., Steiger, M.H., Trentacoste, N., 1966. "Studies on three-dimensional viscous jets". AIAA Journal 4, 800–806. doi:10.2514/3.3549.

Shields, B., Neroorkar, K., Schmidt, D., 2011. "Cavitation as Rapid Flash Boiling", ILASS-Americas 23rd Annual Conference on Liquid Atomization and Spray Systems.

Soteriou, C., Andrews, R., Smith, M., 2010. "Direct Injection Diesel Sprays and the Effect of Cavitation and Hydraulic Flip on Atomization". SAE Technical Paper Series 1. doi:10.4271/950080.

Sun, Z.Y., Li, G.X., Chen, C., Yu, Y.S., Gao, G.X., 2015. "Numerical investigation on effects of nozzle's geometric parameters on the flow and the cavitation characteristics within injector's nozzle for a high-pressure common-rail di diesel engine". Energy Conversion and Management 89, 843–861. URL: http://dx.doi.org/10.1016/j.

enconman.2014.10.047, doi:10.1016/j.enconman.2014.10.047.

Tamaki, N., Shimizu, M., Hiroyasu, H., 2001. "enhancement of the atomization of a liquid jet by cavitation in a nozzle hole". Atomization and Sprays 11.

Taub, G.N., Lee, H., Balachandar, S., Sherif, S.A., 2013. A direct numerical simulation study of higher order statistics in a turbulent round jet. Physics of Fluids 25. doi:10.1063/1.4829045.

Trentacoste, N., Sforza, P., 1967. "Further experimental results for three- dimensional free jets". AIAA Journal 5, 885–891. doi:10.2514/3.4096.

Vallet, A., Borghi, R., 1999. "Modelisation eulerienne de l'atomisation d'un jet liquide". Comptes Rendus de l'Academie de Sciences - Serie IIb: Mecanique, Physique, Chimie, Astronomie 327, 1015–1020. doi:10.1016/S1287-4620(00)87013-1.

Vallet, A., Burluka, A.A., Borghi, R., 2001. "Development of a Eulerian model for the atomization of a liquid jet". Atomization and Sprays 11.

Wakuri, Y., Fujii, M., Amitani, T., Tsuneya, R., 1960. "Studies on the Penetration of Fuel Spray in a Diesel Engine". Bulletin of JSME 3, 123–130. URL: http://joi.jlc.jst.go.jp/JST.Journalarchive/jsme1958/3.123?from=CrossRef, doi:10.1299/jsme1958.3.123.

Wang, Y., Lee, W.G., Reitz, R.D., Diwakar, R., 2011. "Numerical Simulation of Diesel Sprays Using an Eulerian-Lagrangian Spray and Atomization (ELSA) Model Coupled with Nozzle Flow", in: SAE Technical Papers. URL: https://www.sae.org/content/2011-01-0386/, doi:10.4271/2011-01-0386.

Xue, Q., Battistoni, M., Powell, C.F., Longman, D.E., Quan, S.P., Pomraning, E., Senecal, P.K., Schmidt, D.P., Som, S., 2015. "An Eulerian CFD model and X-ray radiography for coupled nozzle flow and spray in internal combustion engines". International Journal of Multiphase Flow 70, 77–88. doi:10.1016/j.ijmultiphaseflow.2014.11.012.

Yakhot, V., Smith, L.M., 1992. "The renormalization group, the eps-expansion and derivation of turbulence models". Journal of Scientific Computing 7, 35–61. doi:10.1007/BF01060210.

Yu, S., Yin, B., Deng, W., Jia, H., Ye, Z., Xu, B., Xu, H., 2018. "Experimental study on the spray characteristics discharging from elliptical diesel nozzle at typical diesel engine conditions". Fuel 221, 28–34. doi:10.1016/j.fuel.2018.02.090.

Yunyi, G., Changwen, L., Yezhou, H., Zhijun, P., 1998. "An experimental study on droplet size characteristics and air entrainment of elliptic sprays". SAE Technical Papers doi:10.4271/982546.

Zhao, H., Quan, S., Dai, M., Pomraning, E., Senecal, P.K., Xue, Q., Battistoni, M., Som, S., 2014. Validation of a Three-Dimensional Internal Nozzle Flow Model Including Automatic Mesh Generation and Cavitation Effects. Journal of Engineering for Gas Turbines and Power 136. URL: https://doi.org/10.1115/1.4027193, doi:10.1115/1.4027193.